

Thermodynamically Stable Colloidal Solids: Interfacial Thermodynamics from the Particle Size Distribution

Andrew Nelson^{†*} and Lawrence H. Friedman[‡]

Materials Measurement Science Division, National Institute of Standards and Technology
100 Bureau Drive, Gaithersburg, MD 20899

[†]ORCID: 0000-0002-2635-8612

[‡]ORCID: 0000-0003-2416-9903

* Corresponding author. Email: nelson.andrew.wm@gmail.com

Abstract

True thermodynamic stability of a solid colloidal dispersion is generally unexpected, so much that thorough experimental validation of proposed stable systems remains incomplete. Such dispersions are underinvestigated and would be of interest due to their long-term stability and insensitivity to preparation pathway. We apply classical nucleation theory (CNT) to such colloidal systems, providing a relationship which links the size-dependent interfacial free energy density of the particles to their size distribution, and use this expression in the fitting of previously reported size distributions for putatively thermodynamically stable nanoparticles. Experimental data from a gold-thiol system exhibiting inverse coarsening or “digestive ripening” can be well-described in terms of a power-law dependence of the interfacial free energy γ on radius based on capacitive charging of the nanoparticles, going as r^{-3} , as suggested by prior authors. Data from magnetite nanoparticles in highly basic solutions also can be well-fit using the CNT relation, but with γ going as r^{-2} . Slightly better fits are possible if the power of the radius is *non*-integral, but we stress that more complex models of γ will require richer data sets to avoid the problem of overfitting. Some parameters of the fits are still robustly at odds with earlier models that implicitly assumed *absolute* thermodynamic stability: first, the extrapolated free energy density of the flat surface in these systems is small and positive, rather than strongly negative; second, the shape of the distributions indicates the solution phase to be supersaturated in monomer relative to the bulk, and thus that these two systems may only be metastable. For future work, we derive expressions for the important statistical thermodynamic and chemical parameters of the interface energy in terms of 1) the surfactant concentration, 2) the temperature dependence, and 3) the concentrations of particles in the tail of the distribution.

1 Introduction

The physical chemistry of surfaces and interfaces is intimately bound up in the preparation and utilization of colloidal materials. From a fundamental standpoint, characterization of the properties of the tiny regions over which colloids are joined to the surrounding medium poses a major challenge, and the energetics of their formation in complex chemical environments is a subject of great interest. Surface chemistry is also a foundational axis along which the preparation of precise and useful nanostructures is accomplished: in this regard, the synthesis of solid colloidal nanoparticles (or nanocrystals) has been a particularly intense area of research for the past few decades,^{1, 2, 3, 4, 5, 6} with subsequent immense improvements in outcome quality measures such as throughput, functional properties, and product uniformity. Optimization of synthetic processes has primarily proceeded along the lines of controlling the kinetics of nucleation and growth of the particles,^{7, 8, 9, 10, 11} and equilibrium thermodynamics is generally invoked only in providing the driving force for precipitation of the solid or for stabilizing specific crystalline surfaces.^{12, 13, 14} Underlying these priorities is the unspoken assumption that colloidal nanoparticles fall into the class of lyophobic¹⁵ colloids—that is, collections of nanoparticles are inherently unstable and inevitably will aggregate or coarsen to minimize their total surface or interfacial area if they are allowed to exchange mass or contact each other. Such an outcome is undesirable both for displacing distribution of particle sizes from its chosen mean and for broadening that distribution, the latter of which especially conflicts with demands^{16, 17, 18, 19} on the narrowness (monodispersity) of colloidal particle ensembles.

Syntheses in which this restriction is lifted, i.e., where nanoparticle solutions can be made thermodynamically stable, would have obvious advantages, most especially in providing dispersions of indefinite lifetime on any scale with no regard to the path taken to the equilibrium state. The chemical theory involved with the future designs of such a synthesis has a well-studied basis in the formalism of classical nucleation theory (CNT). We will apply CNT, in its role of calculating the equilibrium population of particles of a given size, to systems of solid colloidal particles with the goal of measuring interfacial thermodynamics through the correspondence of a size-dependent interfacial free energy density (often called “surface energy”) to an experimental particle size distribution. CNT provides an analytical form of the particle size distribution that can be inverted to instead write the effective excess interfacial free energy, γ , as a function of nanoparticle radius from a measured size distribution. Application of this expression to assumed size distributions illustrates the effects most importantly, how the polydispersity of the size distribution depends on the mechanism underlying the size dependence of γ . We will analyze experimentally measured size distributions reported in previous works, specifically the organic-phase gold-thiol-toluene system (widely used in “digestive ripening”)²⁰ and the aqueous-phase magnetite-hydroxide system.²¹ In this analysis we ascertain the goodness of fit for the CNT-motivated model and its assumed form, infer the chemical model giving rise to the size-dependent γ in colloidal systems, and, in fact, whether these experiments actually characterize thermodynamically stable colloidal dispersions. Finally, from the analytical form of the particle size distribution we derive relationships between the surfactant concentration or temperature and size distribution that are of use in measuring physicochemical parameters of the system, and we provide special or limiting approximations of the size distribution that probe parameters that would otherwise need to be assumed, such as the statistical-mechanical model of the so-called replacement free energy in CNT.

Many works—though far fewer than for kinetically controlled approaches, perhaps indicating the principal difficulty is identifying such systems in the first place—have observed colloidal dispersions of nanometer-size solid particles that meet some or all of the key criteria for thermodynamic stability: long or indefinite system life, spontaneous breakdown of larger particles and coalescence of smaller ones into a population of a single mean size,^{22, 23, 24} and independence of preparation conditions.²⁵ These phenomena have been observed, or been proposed to appear, for a many kinds of solids (including metals^{20, 26, 27} and semiconductors^{28, 29, 30}), and the terms inverse Ostwald ripening or digestive ripening^{31, 32, 33, 34} occur frequently for systems which especially satisfy the first (spontaneous breakup) criterion. A universal feature of these syntheses is the presence of an excess of surface-binding molecules (surfactants). This is analogous to the extensively-studied case of microemulsions, which consist of droplets of one liquid dispersed in another with the aid of one or more surfactant(s): the surfactant lowers the interfacial free energy, γ , by the free energy of adsorption, to a point where it becomes energetically favorable for small domains of one phase to be dispersed in the surrounding medium through the entropic free energy of mixing of the particles with the medium.^{35, 36, 37} Likewise, a colloidal solution with a distribution of particle sizes—a polydisperse colloid—is entropically preferred over a

monodisperse (single-sized) colloid, by way of the mixing entropy.³⁸

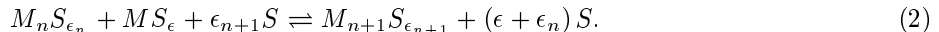
Thermodynamically stable colloidal dispersions are characterized by a mean radius in the nm range, having a relatively narrow distribution about this mean with few very small or very large particles. In some cases the distributions can be nearly monodisperse; from a perspective of nanoparticle synthesis, this criterion is usually set as a standard deviation of the radius 5% or less of the mean.² A sharply peaked distribution with mean far from molecular size requires an intrinsically size- (curvature-) dependent value of the interfacial free energy density, specifically one where γ increases as the particles become smaller.^{36, 15, 39} It has been understood for many years⁴⁰ that γ should in general be dependent on the curvature of the surface or interface, i.e., the particle size r , though why γ changes and what sign $d\gamma/dr$ takes will obviously be system-dependent. In the cases of colloidal nanoparticles, microemulsions, and other dispersed nanostructures, several candidate mechanisms for increasing γ with decreasing r have been nominated. These include the energy needed to form an electrical double layer in an electrolyte solution,³⁶ to charge particles in a dielectric medium,⁴¹ to bend organic monolayers coating the colloid or droplet,^{42, 39} or to polarize plate- or wire-like nanostructures with polar crystal faces.^{24, 43}

Although several systems have been proposed, one of the most salient observations upon a cursory overview of previously published results in purportedly thermodynamically stable colloidal solids is the absence of unambiguous tests of thermodynamic stability, that is, the ability to have the system return to its initial state after the external variables are restored following large incursions in temperature, solid concentration, pressure, and so on. True demonstrations of reversibility are not common^{24, 44} and have been to our knowledge restricted to highly anisotropic samples for which our analysis will require further development. Our work provides a route to answer the thorny question of whether true thermodynamic stability has been observed in the experiments we analyze here, and sets forth firm guidelines in the future for how such distributions should behave. In these experiments, proper confirmation of the domains of stability for such colloids will also inform the development of synthetic procedures for dispersions that are reproducible and resistant to contamination and degradation over time. The goal of such preparations will be not only to measure interfacial energetics but to tailor the size-dependent behavior of γ to make the limiting polydispersity as small as possible.

The basis of our description of the limiting polydispersity is classical nucleation theory, which gives the size distribution of disperse systems according to the dynamic equilibrium of the coupled series of chemical reactions for n ranging from 1 to ∞ ,



where M_1 is called a monomer and M_n is an aggregate of n monomers. In a typical colloid system, this will represent the reaction of monomer complexes of the formula M_1S_ϵ —monomer solvated by ϵ surface-active molecules (surfactants, ligands, or adsorbates) S —with a colloidal nanoparticle $M_nS_{\epsilon_n}$ having n monomers and ϵ_n surfactant molecules to form a larger nanoparticle $M_{n+1}S_{\epsilon_{n+1}}$:



Any colloidal nanoparticle $M_nS_{\epsilon_n}$ corresponds to the following equilibrium:



At the minimum of the Gibbs free energy of the system G given conserved amounts of monomer and surfactant in the system, the chemical potential μ_n of a particle of size n with ϵ_n surfactant molecules depends only on the chemical potentials of monomers and surfactants μ_1 and μ_s :

$$\mu_n = n\mu_1 + (\epsilon_n - n\epsilon)\mu_s. \quad (4)$$

The chemical potential of any component i is of the form $\mu_i = \mu_i^0 + kT \ln a_i$, where μ_i^0 is a standard state chemical potential, k is Boltzmann's constant, and a_i is the thermodynamic activity. Because a_i is directly proportional to the number of colloidal particles N_n (in dilute solutions, as we consider here, the proportion is the Henry's law constant),⁴⁵ Equation 4 can be solved for N_n in terms of μ_1 and μ_s , which become experimentally adjustable parameters that fix the size distribution. Hence, the absolute concentration of particles of each size at equilibrium can be determined given knowledge of the form of μ_i^0 and a_i from statistical

mechanics, and each such relatively large nanoparticle might be termed a lyophilic colloid.⁴⁶ The classical theory of nucleation has been developed for this purpose over the past century^{47, 48, 49, 50, 51, 52, 53, 54, 55} explicitly to calculate the N_n of aggregates, droplets, or colloidal particles of a given number of monomers n at equilibrium, and has reached a high level of technical sophistication. Although the theory of the kinetics of nucleation has to some extent set aside the notion of an equilibrium size distribution providing the nuclei for the growth of new phases, given the inherently non-equilibrium nature of nucleation,^{56, 57, 58, 59, 60} thermodynamically stable dispersions of solids and liquids proposed in other contexts should possess the equilibrium character for which CNT would be a good statistical thermodynamic approach. It is important to emphasize that this equilibrium part of CNT follows from very general thermodynamic principles, and that the condition of thermodynamic stability avoids the need to make (very difficult) predictions of process rates. The most important conclusion of CNT for the equilibrium state is that N_n , for n significantly larger than 1, should be of the analytical form

$$N_n = \alpha n^\beta \exp \left[-\frac{\gamma}{kT} r^2 \right] \exp \left[\frac{\Delta\mu}{kT} n \right], \quad (5)$$

where α and β are constants that depend on the statistical-mechanical model, γ is again the excess interfacial free energy density, r is a characteristic dimension proportional to $n^{1/3}$ such as the radius of a sphere, and $\Delta\mu$ is the difference in the chemical potentials of bulk versus solvated monomer (i.e., the degree of under- or supersaturation). Various authors have derived values for β ranging from 0 to 4.^{49, 61, 62, 54} The sum of N_n over all n parallels the partition function of a single aggregate, droplet, or particle at fixed chemical potential (of monomer) and temperature (μT ensemble) as described by the thermodynamics of small systems.^{63, 64} Eq. 1 makes clear the exact correspondence between an observed equilibrium distribution (usually measured as the probability distribution $p(r)$, in terms of particle radius r) and the excess interfacial free energy given knowledge of β and the differences in component chemical potentials. We propose to use this relationship to derive γ from the observed concentration of nanoparticles as a function of particle radius, $Np(r)$ (N is the *total* number of nanoparticles $\sum_n N_n$), in two proposed cases of thermodynamically stable solid nanoparticles. To this end, we demonstrate in Section 3 how the different forms of Eq. 5 and models for size-dependent γ will be reflected in experimental data, and give for future exploration equations that can make use of higher-precision data on nanoparticle size distributions.

The combination of these thermodynamic expressions with existing data on molecular solubility and measurements or theoretical calculations of interface energies will provide a sounder basis for targeted design of thermodynamically stable solid dispersions. Finally, application of Eq. 5 to some experimental data on solid dispersions in the colloidal nanocrystal literature makes clear that, although good fits to the apparent r - γ relation can be made with few parameters, at present the resolution of those measurements (particle-size histograms) is lacking in its ability to discriminate between different statistical-mechanical assumptions underlying CNT. Nonetheless, the agreement of the size-distribution data from gold-thiol and magnetite-hydroxide systems with the CNT-derived expressions is excellent. With some auxiliary assumptions, they could indicate a power-law dependence of γ on r with a non-integer exponent, which is not anticipated by some simple models for γ ,^{41, 32} but descriptions with an integer exponent are also semiquantitatively reasonable. Future work, at least for the systems considered here, must still assure that the necessary criteria for these assumptions are satisfied in order to make mechanistic judgments such as establishing the existence of a spontaneous curvature of the solid-solution interface.

2 Theory

First, we will recapitulate the relevant arguments of CNT and adapt them to our systems. According to Eq. 4 the chemical potential of any aggregate or nanoparticle size, μ_n , can be specified precisely in terms of the chemical potentials of the smallest components, monomer and surfactant. We will henceforth refer strictly to (nano)particles, treating them as single (very large) molecules. The statistical-mechanical definition of the

chemical potential is

$$\begin{aligned}\mu_n &= \left(\frac{\partial A}{\partial N_n} \right)_{T,V,N_x} \\ &= kT \left[\ln \frac{N_n}{q_n} + \sum_x N_x \left(\frac{\partial \ln q_x}{\partial N_n} \right)_{T,V,N_x} \right],\end{aligned}\quad (6)$$

where A is the Helmholtz free energy of the system and q_n is the canonical partition function of the particle of size n . The variable x indicates a component other than nanoparticles (solvent, surfactant, etc.). In ideal gases or in dilute solutions where the energy of solvent-nanoparticle interactions can be assigned solely to the interfacial energy γ due to the absence of inter-particle collisions, the second term in the sum is zero, but q_n is an *effective* partition function which includes the averaged interactions with the exterior liquid phase of solvent, surfactant, and monomer (giving rise, e.g., to the Henry's law constant).⁴⁵ Substituting Eq. 6 into Eq. 4 and rearranging terms gives the size distribution:

$$N_n = q_n e^{\frac{n\mu_1}{kT}} e^{\frac{(\epsilon_n - n\epsilon)\mu_s}{kT}}. \quad (7)$$

This expression is similar in form of a partition function in the fully open (μ_1, μ_s, T or μ_1, μ_s, p, T) ensembles, as described by the thermodynamics of small systems.⁶³ In effect, an ensemble of single particles is placed in contact with reservoirs of monomer and surfactant, and the value of N_n reflects the probability a particle will have a particular size. Although nonzero values of $\partial \ln q_x / \partial N_n$ in Eq. 6 spoil this definition, we estimate their effects for the case of interparticle interactions where the chemical potential has an ideal component, $\mu_n^{(id)}$, and an excess component, $\mu_n^{(ex)}$, in Section 2.3.

Note that here we will use N_n interchangeably with the concentration of nanoparticles in one cubic meter (that is, the volume of the system $V = 1 \text{ m}^3$).

2.1 Choice of prefactor in the nanoparticle partition function

The partition function q_n in Eq. 7 is formulated as the product of external and internal partition functions, respectively $q_n^{(ext)}$ and $q_n^{(int)}$:

$$q_n = q_n^{(ext)} q_n^{(int)},$$

where the internal partition function is defined with respect to the Gibbs free energy of a stationary nanoparticle, $G_n^{(int)}$,

$$q_n^{(int)} = \exp \left(- \frac{G_n^{(int)}}{kT} \right), \quad (8)$$

which is, including a term for the surfactant molecules,

$$G_n^{(int)} = n\mu_b + \epsilon_n \mu_s^* + 4\pi r^2 \gamma \quad (9)$$

where μ_b is the chemical potential of a monomer in the bulk phase, μ_s^* is the chemical potential of a surfactant molecule bound to a flat interface at a certain reference chemical potential of the surfactant, μ_s , in the solution phase, and r is the particle (core) radius $(3n/4\pi\rho_b)^{1/3}$, with ρ_b being the molecular density of monomers in the bulk. Two notes are warranted. Because this work deals with solids, it is important briefly to distinguish between the surface free energy or surface tension and the surface stress, which are non-equivalent in solids.⁶⁵ Here we specifically refer to the surface free energy, or the work of formation of new surface, which the appropriate parameter determining the change of the chemical potential of the single component inside the nanoparticle core.⁶⁶ Second, $q_n^{(int)}$ should be a function of the Helmholtz free energy of the nanoparticle, rather than the Gibbs free energy, the difference being the pressure-volume product $-pV_n$ where V_n is the particle volume. An assumption common to CNT regarding $G_n^{(int)}$ is that the colloid is effectively incompressible, regardless of the Laplace pressure from the surface tension or free energy, so that the Helmholtz and Gibbs

free energies are equal. A qualitative estimate is provided in Section S2 of the Supporting Information of the work done in compressing an Au particle core from its undilated state, with energy due to the pressure-volume product pV_n , to a compressed state with product $p'_n V'_n$, with the assumption of a small deformation elasticity, for conservative (large) values⁶⁷ of γ . The correction due to the finite compressibility of the core is found to be negligible, with a correction to γ of order 10^{-3} or less, even though the value of γ used is for a *clean* solid surface rather than a surfactant-protected one. Thus, we apply in Eq. 6 what is essentially the capillarity approximation,⁵⁰ with the exception that γ is now a fitting parameter that only has as a component the interfacial free energy density of a flat surface.

With the internal part defined, the external part $q_n^{(ext)}$ accounts for the motion of the nanoparticle throughout the medium (vapor or liquid), which is not possible when its components are embedded in the bulk. Since $G_n^{(int)}$ includes contributions from all degrees of freedom of the constituent molecules of the nanoparticle, $q_n^{(ext)}$ consists of a partition function describing the extracted degrees of freedom associated with free particle motion, $q_n^{*(ext)}$, which is canceled by dividing by a replacement partition function, $q_n^{(rep)}$:

$$q_n^{(ext)} = \frac{q_n^{*(ext)}}{q_n^{(rep)}}. \quad (10)$$

Combining Eqs. 7–10 obtains

$$\begin{aligned} N_n &= q_n^{(ext)} e^{-\frac{G_n^{(s)}}{kT}} e^{\frac{n\mu_1}{kT}} e^{\frac{(\epsilon_n - n\epsilon)\mu_s}{kT}} \\ &= q_n^{(ext)} \exp \left[\frac{n(\mu_1 - \mu_b - \epsilon\mu_s) + \epsilon_n(\mu_s - \mu_s^*) - 4\pi r^2 \gamma}{kT} \right]. \end{aligned} \quad (11)$$

The argument of the exponent is understood in CNT to be the reversible work of formation of a stationary nanoparticle from its component monomers and surfactant molecules. The term $\mu_s - \mu_s^*$ in Eq. 11 is recognizable from the Gibbs adsorption equation. We will assume throughout this work that the maximum surfactant binding density ϵ_0 is independent of particle size. $\epsilon_n = 4\pi r^2 \epsilon_0$ when the surface is saturated with surfactant, so γ can be written as an effective interfacial free energy density $\gamma^* = \gamma + \epsilon_0(\mu_s - \mu_s^*)$. Where particles with *unsaturated* surfactant shells must be considered, N_n is a function N_{ij} of both the number of monomers i and surfactant molecules j , but such cases are unlikely to be relevant for our purposes. i and j (and so on) may also be any other quantities related to size and composition, for example the length and diameter of a rod-shaped particle or the number of monomers along with the number of elementary charges. Here, we will retain our assumption of spherical shape and consider only a constant site density ϵ_0 . This, along with defining $\Delta\mu = \mu_1 - \mu_b - \epsilon\mu_s$, gives us the size distribution expression that we will use in our analysis of experimental data:

$$N_n = q_n^{(ext)} \exp \left[\frac{n\Delta\mu - 4\pi r^2 \gamma^*}{kT} \right]. \quad (12)$$

In applying this equation to our data, we will need to choose a form for the size dependence of γ^* , so that there are at least three undetermined parameters in the exponent, plus a choice that needs to be made for $q_n^{(ext)}$. Of interest is that the identity of the monomer is irrelevant, with the chemical potentials of all products and reactants except the particle buried in $\Delta\mu$. At equilibrium between monomer and bulk solid, so that $\mu_b + \epsilon\mu_s = \mu_1$, this also disappears. In the case of nucleation from vapors, this corresponds to the state at the boiling point; in the case of microemulsions, this corresponds to the Winsor I or II states in which a globular dispersion exists in equilibrium with a bulk phase of the dispersed component.⁶⁸ As indicated previously, however, in the experiments we consider here this equilibrium cannot be assumed.

We delimit a number of approaches for writing down the prefactor, $q_n^{*(ext)}/q_n^{(rep)}$, which produce very different dependences on n and overall magnitude. A notable one from Lothe and Pound⁴⁹ is to write the partition function of the particle as the product of translational, rotational, and vibrational partition functions, here identified by superscripts (t) , (r) , and (v) , respectively:

$$q_n = q_n^{(t)} q_n^{(r)} q_n^{(v)}$$

The translational and rotational partition functions are given by their ideal-gas forms in the semiclassical approximation: the rotational and translational partition functions for “nearly” spherical particles (symmetry number of unity, but with all moments of inertia equal) moving freely throughout the system are⁴⁵

$$q_n^{(t)} = V \left(\frac{2\pi m_n kT}{h^2} \right)^{3/2} \quad (13)$$

$$q_n^{(r)} = 8\pi^2 \left(\frac{2\pi I_n kT}{h^2} \right)^{3/2}, \quad (14)$$

where m_n is the mass of a nanoparticle with n monomers and I_n is its principal moment of inertia. Here we have assumed the particles are “nearly” spherical, having all three moments of inertia equal as well as a symmetry number of unity. $q_n^{(v)}$ is the product of the vibrational partition functions for the modes with frequency ν associated with the $3n - 6$ degrees of freedom remaining to the particle:

$$q_n^{(v)} = \prod_i^{3n-6} \frac{kT}{h\nu_i}$$

The replacement partition function, $q_n^{(rep)}$, is that which produces $q_n^{(rep)} q_n^{(v)} = \exp \left[-G_n^{(int)}/kT \right]$. That is,

$$q_n^{(ext)} = \frac{q_n^{(t)} q_n^{(r)}}{q_n^{(rep)}}. \quad (15)$$

Eq. 15 is also called the Frenkel factor.⁵⁴ Lothe and Pound estimated $q_n^{(rep)}$ to correspond to the entropy of one molecule of a bulk liquid phase, a value of about $5k$, giving $q_n^{(rep)} = e^5$. Although we consider solids here rather than liquids, the value of $q_n^{(rep)}$ does not matter much in this case, because $q_n^{(t)} q_n^{(r)}$ is so large. This quantity is dependent on n as n^4 , and for $n \sim 100$ (a particle radius of 5–10 Å), it is already in the neighborhood of 10^{44-46} , while for radii more typical of nanoparticles (~ 3 nm, $n \sim 5000$) it is around 10^{50-52} .

Reiss, Katz, and Cohen⁶⁹ gave a different treatment of the system by relating $q_n^{(t)}$ instead to the probability density of the center of mass of the stationary particle,

$$P_n(0) = (2\pi)^{-3/2} \sigma_n^{-3}, \quad (16)$$

where the standard deviation of the fluctuations of the center of mass of the n -sized nanoparticle, σ_n , is in the case of dense solids about

$$\sigma_n = 0.147n^{-1/2}V_n^{1/3}. \quad (17)$$

The factor of 0.147 is our estimate based on a filling fraction 0.74 for dense solids. The origin of σ_n lies in the fact that, in considering the translation of the particles in $q_n^{(t)}$, it is the center of the volume V_n that is being moved, rather than the true center of mass, which can fluctuate around that point. The final expression for $q_n^{(ext)}$ is

$$q_n^{(R)} = V P_n(0). \quad (18)$$

$q_n^{(RKC)}$ is smaller than $q_n^{(LP)}$ by many orders of magnitude, being only around 10^{29-31} , and it depends on n only as approximately $n^{1/2}$, a very different exponent (if V_n is the sum of the monomer volumes, then σ above goes as $n^{1/6}$). In relation to Eq. 12, the effect will be to, for the same observed N_n and $\Delta\mu$, reduce the corresponding magnitude of γ^* .

An elaboration on $q_n^{(RKC)}$ was given by Kusaka;⁷⁰ we use here a formula approximated by Vosel, Onischuk, and Purtov.⁵⁴ In effect, rotation is reintroduced by $q_n^{(r)}$, then partly canceled by a factor $q_n^{(r,rep)}$ corresponding to the rotational degrees of freedom for a particle with constrained coordinates. (The definition of $q_n^{(ext)}$ in this manner is based on a statistical-mechanical treatment of a process in which the particle of condensed

phase is drawn out or extruded from the bulk phase; the reader should consult the appropriate references for more details.) The new external partition function is

$$q_n^{(K)} = VP_n(0) \frac{q_n^{(r)}}{q_n^{(r,rep)}}, \quad (19)$$

where $q_n^{(r,rep)}$ is assumed to be the partition functions of harmonic oscillators:

$$q_n^{(r,rep)} = \left[e^{\frac{h\nu_n}{2kT}} \left(1 - e^{-\frac{h\nu_n}{kT}} \right) \right]^{-3}. \quad (20)$$

ν_n is an oscillator frequency which can be approximated by relating it to the Debye frequency of the nanoparticle core, ν_D , such that $\nu_n = \sqrt{3}n^{-1/6}\nu_D$ as described by Lothe and Pound.⁷¹ In solids, $\nu_D = k\Theta_D/h$, where Θ_D is the experimentally measured Debye temperature; alternatively, it may be estimated from simulations. As a result, Eq. 19 has a slightly non-polynomial dependence on n . In the limit of high temperature, it would depend as $n^{5/2}$, but the Debye temperature is generally comparable to or greater than room temperature. (This is the case for the experimental systems we consider below.^{72, 73}) The magnitude of $q_n^{(K)}$ lies somewhere between $q_n^{(RKC)}$ and $q_n^{(LP)}$.

2.2 Alternative external partition function in the solution phase

Although Eqs. 15, 18, and 19 were proposed for vapor-to-liquid nucleation, CNT in solid-liquid or solid-solution systems should (and has been assumed to) follow the same formalism since particles can still move and rotate throughout the entire system on long enough timescales.³⁵ Using a cell theory of liquids and liquid mixtures,⁴⁵ we suggest a fourth external partition function for a nanoparticle residing in an environment in which its local motion is restricted due to the presence of neighboring molecules. The tendency of the molecules to wander through the entire volume of the system over time is described combinatorically by the number of ways to arrange the $N_l + N_s + \sum_n N_n + \dots$ molecules in the system in energetically equivalent configurations. In this way Eq. 12 becomes instead

$$\frac{N_n}{N_l + N_s + \sum_n N_n + \dots} = q_n^{(ext)} \exp\left(\frac{n\Delta\mu - 4\pi r^2\gamma^*}{kT}\right) \quad (21)$$

where the restricted motion of the nanoparticle within its solvent molecule cage defines the accessible phase space volume for $q_n^{(ext)}$. Eq. 21 assumes that the molecules mix according to the ideal mixing law. This strictly holds only in systems of one dimension or for mixtures of chemically identical molecules, but has been observed to remain a reasonable approximation even for molecules of very unequal sizes as long as the species are compact and rigid.^{74, 75, 76} This assumption of rigidity will obviously hold well for colloidal solids.

In defining this fourth external partition function it is important to reiterate that $q_n^{(rep)}$ is formally the product of the partition functions for the six (unknown) vibrational modes, which may be dependent on n , that were removed in defining $q_n^{(t)}q_n^{(r)}$. When a particle is embedded in a medium, it experiences hindered translation and rotation. Where the barriers for translation and rotation are large and the classical approximation remains valid, the partition function of the i th mode is $kT/h\nu_i$, where ν_i is its frequency.⁴⁵ Then, $q_n^{(ext)}$ becomes

$$q_n^{(ext)} = 8\pi^2 e \frac{\prod_{i=1}^6 \nu_{ni}^{(rep)}}{\prod_{i=1}^3 \nu_{ni}^{(t)} \prod_{i=1}^3 \nu_{ni}^{(r)}}. \quad (22)$$

$\nu_{ni}^{(rep)}$ is the i th mode frequency corresponding to “translation” and “rotation” for the n -sized particle as embedded in its parent condensed phase, while $\nu_{ni}^{(t)}$ and $\nu_{ni}^{(r)}$ are the translational and rotational frequencies associated with the n -sized particle in its new medium. The factor of e is a so-called communal entropy⁴⁵ reflecting the energetic equivalence of different arrangements of the molecules in the system, as in the case of an ideal gas, and $8\pi^2$ is an analogous term from the rotational partition function. Thus, at high temperatures it is the n -dependence of the frequencies in Eq. 22 that controls the n -dependence of the prefactor in the size

distribution. Intuitively, $q_n^{(ext)}/8\pi^2e$ should be greater than one when the bulk solid is more rigid than the embedding medium since, e.g., in solution a colloidal particle translates and rotates more freely than when embedded in the bulk. Although it is unlikely that $q_n^{(ext)}$ should be completely n -independent, taking the product/quotient of the vibrational frequencies in Eq. 22 as a constant, $q_n^{(0)}$, is interesting in the context of how γ and N_n are related to each other, as will be detailed in Section 3. Where the solvent molecules greatly outnumber surfactant molecules and colloidal particles, the total number of molecules is roughly the number of solvent molecules N_l , which changes Eq. 21 to

$$N_n = N_l q_n^{(0)} \exp\left(\frac{n\Delta\mu - 4\pi r^2 \gamma^*}{kT}\right) \quad (23)$$

The large value of N_l in any dilute system makes the magnitude of $N_l q_n^{(0)}$ more similar to the prefactors for the models derived for vapor-liquid nucleation even if $q_n^{(0)}$ is very small.

Because the prefactors delimited by Eqs. 15, 18, 19, and 23 span a wide range of values, the predicted absolute concentration of particles in the dispersion can vary by many orders of magnitude depending on the model chosen. If γ is used as a fitting parameter, however, it is rather insensitive to the choice of $q_n^{(ext)}$ since it depends only logarithmically on N_n . As a result, uncertainty in the predicted value of γ makes it much more difficult to determine the prefactor $q_n^{(ext)}$ from a measured N_n . With some approximations, however, information from the tails of the size distribution can indicate the n -dependence of $q_n^{(ext)}$: see Section 3.4. Other pertinent details in calculating $q_n^{(ext)}$ are given in section S3 of the Supporting Information.

2.3 Interparticle interactions

Colloidal particles interact with each other as well as with the solvent, in particular through excluded volume. These interactions contribute an excess term, $\mu^{(ex)}$, to the chemical potential above that of an ideal gas or solution, $\mu^{(id)}$:

$$\mu_n = \mu_n^{(id)} + \mu_n^{(ex)} \quad (24)$$

A simple model for interparticle interactions, which has been already been studied for the case of microemulsions, is the hard-sphere model in which the interaction potential is infinite if two particles overlap and zero if they do not. Accurate expressions for excess free energies of such systems are known and one commonly used one, the Carnahan-Starling equation of state, gives the excess chemical potential per spherical particle solely as a function of the volume fraction ϕ of the colloid. The monodisperse case represents the first-order correction to the free energy of the system, and the excess Gibbs free energy per colloidal particle $\mu^{(ex)}$ is independent of particle size and equal to:⁷⁷

$$\frac{\mu^{(ex)}}{kT} = \frac{8\phi - 9\phi^2 + 3\phi^3}{(1 - \phi)^3}. \quad (25)$$

However, the magnitude of this quantity is extremely small with values of ϕ reflecting the experiments considered, which are of order 10^{-3} or less. This is orders of magnitude smaller than any expected contribution from the interfacial free energy or the entropic motion of the particles, which are in of order $10kT$ (see below). It might be expected to contribute meaningfully for very highly concentrated dispersions, but we are not aware of any prior demonstration of such a concentrated thermodynamically stable suspension.

Furthermore, $\mu^{(ex)}$ should be expected technically to be a function of r . The extension of hard-sphere equations of state to polydisperse systems has also been formulated.⁷⁷ The resulting size-dependent excess free energy was cast in terms of the raw moments of the size distribution $Np(r)$, $M_i = N \int_0^\infty r^i p(r) dr$, where i is the order of the moment. $\mu^{(ex)}$ is a function F of the particle size and the moments up to order three (note that $M_0 = N$ and $M_3 = \frac{3\phi}{4\pi}$),

$$\mu^{(ex)} = F(r, M_0, M_1, M_2, M_3),$$

which in the monodisperse limit reduces to Eq. 25. Numerical examination, described in more detail in Section S4.1 and Figure S1 of the Supporting Information for the exposition given by Salacuse and Stell,⁷⁸ shows

these second-order effects are even smaller than the first-order corrections from the monodisperse hard-sphere model (a few percent; Figure S1a-b), although they nominally favor broadening of the distribution (Figure S1c). Beyond hard-sphere models, the description of $\mu_n^{(ex)}$ is, of course, more complicated. Interactions between nanoparticles can be substantial and extend well beyond the nanoparticle surface.^{79, 80, 81} Previous work on, for example, digestive ripening, has focused on surfactant-solid stoichiometry and not primarily the overall concentration of these components in their solvent. Absent any intuition beyond the simplest models on why certain particle sizes might be disfavored purely on the basis of their interactions with other particles, and knowing for experimentally relevant cases that first, ϕ is very small, and second, the distributions concerned are relatively narrow (and the narrower the better), further work on how the shape of the size distribution changes with interparticle interactions is left for future investigation. For the interested reader, we have included in Section S4.2 an estimate, based on the magnitude of the second virial coefficient, for the strengths of interparticle interactions based on van der Waals attractions,⁸² steric repulsion between surfactant shells,^{83, 81} and electrical double-layer repulsion from the Derjaguin-Landau-Verwey-Overbeek (DLVO) theory.⁸⁴ These interactions were parameterized based on conservative values taken from systems similar to those in Section 3. They show that, while nanoparticles may exclude a volume around them several times that of their nominal hard-sphere size, the resulting increase in effective volume fraction should not increase $\mu^{(ex)}$ to the point where it contributes significantly to the size distribution.

Based on a worst-case scenario outlined in Section S4.1 of the Supporting Information of an effective $\phi = 0.1$ (Figure S1a) we can say that even if the *effective* volume fraction in the experimental cases considered in Section 3 were more than 10-100 times their values estimated by microscopy, the resulting contribution from $\mu^{(ex)}$ would still be small (Figure S1c-d). That is, with $\phi = 0.1$, $\mu^{(ex)} \approx kT$ in the monodisperse case, as compared to the ideal gas term $\mu^{(id)} \approx -33.7kT$ and/or the interfacial energy term $-4\pi r^2\gamma \approx -19kT$, for gold nanoparticles of radius $r = 2.5$ nm with a γ of 1 mJ m⁻². We thus neglect interparticle interactions in our consideration of experimental data in Section 3.

2.4 Form of γ

From Eq. 12, it is clear that, if the magnitude of γ^* in the limit of flat surfaces is negative, the size distribution expression converges only if $\Delta\mu < 0$, i.e., the monomer phase is undersaturated relative to the bulk phase. This indicates, moreover, that bulk and colloidal matter cannot coexist at equilibrium in systems with such values of γ^* . A value of $\Delta\mu$ significantly less than zero was assumed in the models of Whetten and Gelbart⁸⁵ and Manzanares et al.⁴¹. Technically, the supersaturation term can be absorbed into γ if the geometry of the nanoparticle is assumed (for example to be spherical):

$$\frac{4\pi r^3 \rho}{3kT} \Delta\mu = -\frac{4\pi r^2}{kT} \left(-\frac{\rho\Delta\mu}{3} r \right). \quad (26)$$

This term is linear in r . With the understanding that as discussed in Section 1 that the intrinsic size dependence of γ should follow a power law, we can condense the terms of the exponential in Eq. 12 to a generic equation of the following form suitable for fitting to experimental data:

$$\gamma^{**} = ar^b + \delta r + \gamma_0. \quad (27)$$

The constants a , which has units of energy per length to the $b - 2$ power, and b , which is dimensionless, are characteristic of a particular mechanism that affords a size-dependent excess free energy to a colloidal particle, normalized by the particle surface area. δ , which has units of energy per volume, is characteristic of volume-proportional terms such as the degree of supersaturation $\Delta\mu$ per monomer in the nanoparticle. Finally, γ_0 corresponds to the limit of the interfacial energy density for very large particles or flat surfaces, and includes the lowering of γ for the clean surface by adsorbed molecules. Combining Eq. 12 with Eq. 27, the particle size distribution can be written in its most general form (here as a function of r instead of n)

$$Np(r) = \alpha r^\beta \exp \left[-\frac{4\pi r^2}{kT} (ar^b + \delta r + \gamma_0) \right], \quad (28)$$

so there are four undetermined variables for use in nonlinear regression, and the constants α and β are fixed by the choice of $q_n^{(ext)}$ (note that for the same partition function α and β are different when working in r

or in n). Some general conclusions can be drawn from Eq. 27 with little reference to physical parameters. Kegel and Reiss already showed³⁹ that this expression cannot give rise to an equilibrium size distribution with a significant maximum radius (more than 1 nm) without invoking physically implausible values of β if b and δ are zero, i.e. the interfacial energy is constant. We complement this by showing in Section S5 of the Supporting Information that size distributions cannot realistically be *narrow* if γ is independent of radius. Essentially, the polydispersity, like the mean radius, is a function only of β and not of γ_0 , and for the forms of $q_n^{(ext)}$ discussed previously it can be approximately 19% at best, compared to the criterion of “monodisperse” taken to be 5%. The situation is less obvious where $\delta \neq 0$, since the integral of Eq. 28 can no longer be represented in terms of standard functions, but we will find that, for physically reasonable systems, the value of δ has little effect on the polydispersity.

3 Results and Discussion

Eq. 28 can be inverted to give an effective size-dependent interfacial free energy, γ^{**} (Eq. 27), in terms of the size distribution, subject to a choice of $q_n^{(ext)}$. Relevant parameters for our calculations are given in Section S1 and Tables S1–S2 in the Supporting Information. Figure 1 illustrates the dependence of γ^{**} on that choice for a hypothetical population of colloidal Au particles with dodecanethiol surfactant having a normal distribution of radii with mean radius 3 nm and standard deviation 0.3 nm (polydispersity of 10%). In Figure 1a are shown curves of the γ^{**} corresponding to a particular form of $q_n^{(ext)}$ that would all give rise to the same distribution shown in Figure 1b; Figure 1c shows the projections of Figure 1a on an expanded scale. Full curves (and their extensions) correspond to the $q_n^{(ext)}$ in Eqs. 15, 18, and 19, for which quantitative estimates can be provided. With regards to $q_n^{(0)}$, we lack the ability to estimate quantitatively the frequencies associated with constrained motion in the liquid or parent bulk phase as shown in Eq. 22. Therefore, we are restricted to working with arbitrary quantities for illustrative purposes. Figure 1 shows with the dashed lines instead the effects of changing only a constant prefactor arbitrarily or of dictating the relative frequencies of the modes in the numerator and denominator in Eq. 22. We have set the numerator and denominator to be functions of a single frequency ν and ν' respectively, i.e., $\prod \nu_{ni}^{(rep)} = \nu'^6$ and $\prod \nu_{ni}^{(r)} \prod \nu_{ni}^{(t)} = \nu^6$. From a physical perspective, a solid colloidal particle in a less rigid environment is represented by the situation $\nu'/\nu > 1$. The more compliant the environment, the softer the vibrational mode corresponding to the motion of the particle in its cell becomes compared to the same mode for the particle in the bulk solid. The labels of the broken curves labeled $q_n^{(0)}$ in the figure are given by the value of $(\nu'/\nu)^6$ used for a particular curve.

For illustrative purposes, only the segments of γ^{**} lying in a radius range up to three standard deviations from the mean are shown for the full lines in Figure 1a. Beyond this range, the concentration of particles will be extremely small, so typical microscopy measurements which only count up to several hundred particles will have few, if any, measurements in this range. As we discuss in Sections 3.1–3.2, the experiments we consider here reported fat-tailed distributions skewed toward large r , and were not well-described by a normal distribution, but even so less than 1% of the estimated measurements fell outside this three-standard-deviation window. The truncated range available to microscopy measurements has ramifications for the conclusions that can be drawn regarding the form of γ^{**} : the power-law forms of γ mentioned previously are monotonic in r if $\Delta\mu \leq 0$, while the extrapolated curves of γ^{**} have an observable minimum for $q_n^{(RKC)}$, $q_n^{(K)}$, and, depending on the exact value of the prefactor, $q_n^{(0)}$. This minimum falls outside the “observable” range for nanoparticle size distributions if the prefactor is not small enough, as it is for $q_n^{(K)}$. The existence of non-monotonicity is important because, where γ^{**} increases for both small and large r , it is an unambiguous indication that either the solution exists in a state undersaturated in monomer with respect to bulk solid or, more interestingly, that the solid-solution interface has an intrinsically preferred curvature. Although such a favored radius in the nanometric range has been discussed for microemulsions, on the basis of steric constraints,⁸⁶ it has not to our knowledge been considered for nanoparticles.

In addition to the choices of prefactors given by Eqs. 15, 18, 19, and 23, we have included a form of Eq. 23 that drops the factor of N_l that arises from mixing of the colloidal particles throughout the solution. (The other part of the prefactor, $(\nu'/\nu)^6$ above, remains fixed at 10^6 .) A loss of mixing entropy would correspond to a situation in which the particles are no longer freely moving, as would be the case if they were embedded in a solid medium or if thermal motion were insufficient to suspend them against gravity. The

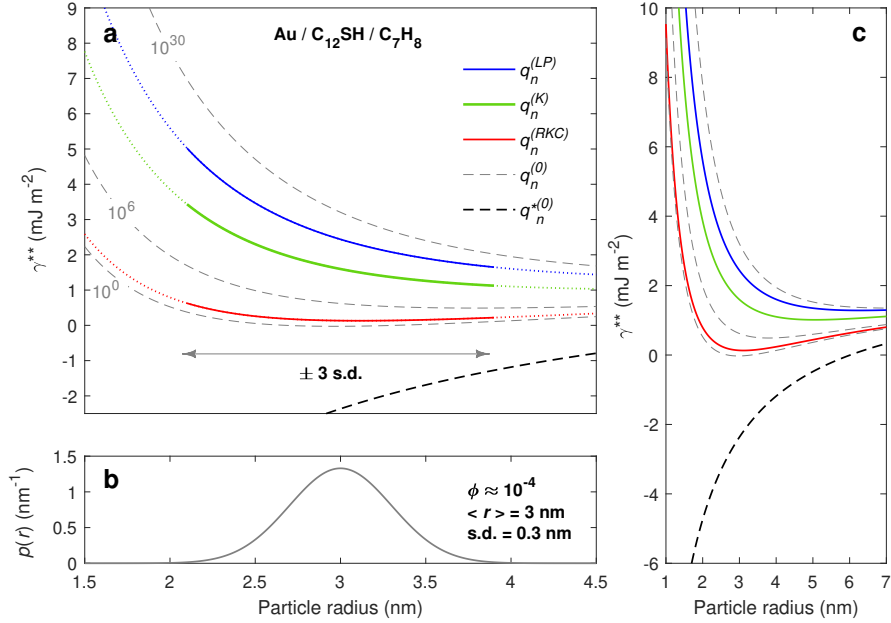


Figure 1. Correspondence between size distribution and interfacial energy for a hypothetical gold-thiol system for four different statistical-mechanical models of the external partition function (a). The light line (b) illustrates the Gaussian size distribution. For clarity, the r - γ^{**} relationship is shown on a larger scale in (c). (LP) Lothe and Pound, Eq. 15; (RKC) Reiss, Katz, and Cohen, Eq. 18; (K) Kusaka, Eq. 19; (0) simple n -independent partition function (this work, Eq. 18). The broken segments of the curves corresponding to $q_n^{(LP)}$, $q_n^{(K)}$, and $q_n^{(RKC)}$ show the extrapolated values of γ more than three standard deviations from the main radius, beyond which observing particles in microscopy experiments is unlikely. Curves labeled $q_n^{(0)}$ are shown with dashed lines labeled by the prefactor used (see main text). Included also (dashed line) is $q_n^{*(0)}$, a modified form of $q_n^{(0)}$ in which the N_l term in Eq. 23 has been removed, representing that the particles no longer move freely in the solution.

latter situation might be the case for previously reported experiments on semiconductor nanosheets^{24, 44} and nanowires.⁴³ This modified external partition function $q_{ext}^{*(0)}$ is interesting, because it shows more clearly that Eq. 12 admits physical solutions in which the effective interfacial free energy in the dominant population of nanoparticles is negative. The stability of such colloidal dispersions is predicated on the existence of some $\Delta\mu$ that makes γ^{**} positive again for sufficiently large r , as seen in the right-hand edge of Figure 1c. It is primarily the magnitude of the constant prefactor that determines the magnitude and sign of γ^{**} , rather than the n -dependence: the logarithm of $q_n^{(ext)}$ contributes $\ln X + Y \ln n$, where X is a constant and Y is the exponent of n . Since Y is probably somewhere from 0 to 4 and n is of order $10^2 - 10^5$ for nanometer-sized particles, $Y \ln n$ contributes relatively little compared to $\ln X$ for the system we have considered in Figure 1. This is also apparent in the near indistinguishability of the dashed curve labeled 10^0 , which is independent of n , from that corresponding to $q_n^{(RKC)}$. A negative value of γ in the limit of zero curvature can be expected to exist in the presence of strongly adsorbing molecules,⁸⁷ so in attempting to isolate such systems we can assert that a major part of their stability should be imposed by restricting their motion, thereby reducing the value of the prefactor that arises from entropic considerations.

In Figure 2, we instead vary the shape of the test distribution by calculating the γ^{**} corresponding to normal distributions of different polydispersities, again in the Au-thiol system. At top are shown the γ^{**} curves, with the prefactor in the size distribution assumed to be from $q_{ext}^{(LP)}$, corresponding to distributions (bottom) with polydispersities of 5%, 10%, and 20%. As in Figure 1, the full lines correspond to ranges of r falling fewer than three standard deviations from the mean. We see immediately that the narrower size distributions are associated with a greater concavity of the r - γ^{**} relationship. Even though the “observability

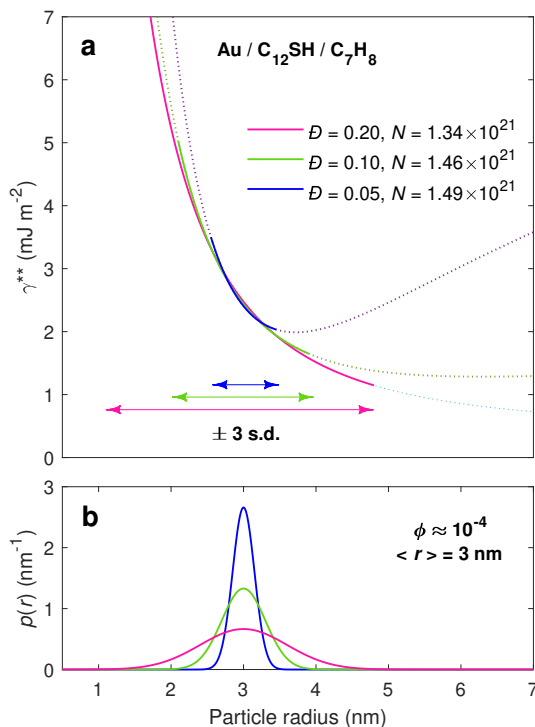


Figure 2. Effects of distribution shape on the effective interfacial energy density γ^{**} (a) for a hypothetical gold-thiol system having nanoparticle radii of mean 3 nm and different polydispersities (b). The broken lines indicate the extrapolated values of γ^{**} more than three standard deviations from the mean radius, beyond which observing particles in microscopy experiments is unlikely.

restriction” means that the non-monotonicity of γ^{**} apparent in the broken lines will be missed in a microscopy experiment, the greater curvature of the interfacial free energy is still apparent in the truncated size range. Nonetheless, the sensitivity of the absolute concentration of colloidal particles to the magnitude of γ^{**} is also apparent, as near the maximum in the size distribution the three curves are barely distinguishable from each other, differing by less than 1%. Because the magnitude of the interface or surface energy in condensed phases is difficult to estimate theoretically, or even to measure to high precision for solids, we can expect from this demonstration that searches for material systems with γ amenable to the observation of thermodynamically stable solid colloidal dispersions are likely to remain empirical for the time being.

In Figure 3 we take the system and distribution in Figure 1, return to the full expression for γ^{**} in Eq. 12, and examine the effect of changing the value of $\Delta\mu$. Additional details are provided in Section S6 of the Supporting Information. Beginning with an assumed normal distribution of radii with $\Delta\mu = 0$ (thick line in Figure 3a), a change in $\Delta\mu$ is equivalent to multiplying this distribution, $Np(r)$, by a factor $\exp n\Delta\mu/kT$, independent of $q_n^{(ext)}$. A negative $\Delta\mu$ (undersaturation with respect to bulk) is equivalent to increasing γ^{**} , while a positive $\Delta\mu$ (supersaturation) is equivalent to lowering γ^{**} , as illustrated in Figure 3b. The values of $\Delta\mu$ are very small, reflecting that colloidal solutions will contain experimentally meaningful concentrations of nanoparticles only very close to the equilibrium between monomer and bulk as a simple result of the law of mass action. This also indicates that the apparent “window of stability” for spontaneously dispersed nanoparticles with regard to temperature is probably very narrow, as the monomeric solubility will depend markedly on temperature; a change in μ for one component of $0.001kT$ translates into a change in concentration of less than 1%. In undersaturated conditions, the size distribution shifts to smaller mean particle sizes (Figure 3a) while the overall particle concentration (Figure 3c) falls exponentially. Conversely, in supersaturated conditions, while from Eq. 12 the number of colloidal particles is infinite regardless of the magnitude of the (nonzero) $\Delta\mu$, a particle size distribution at a finite radius remains metastable, as shown

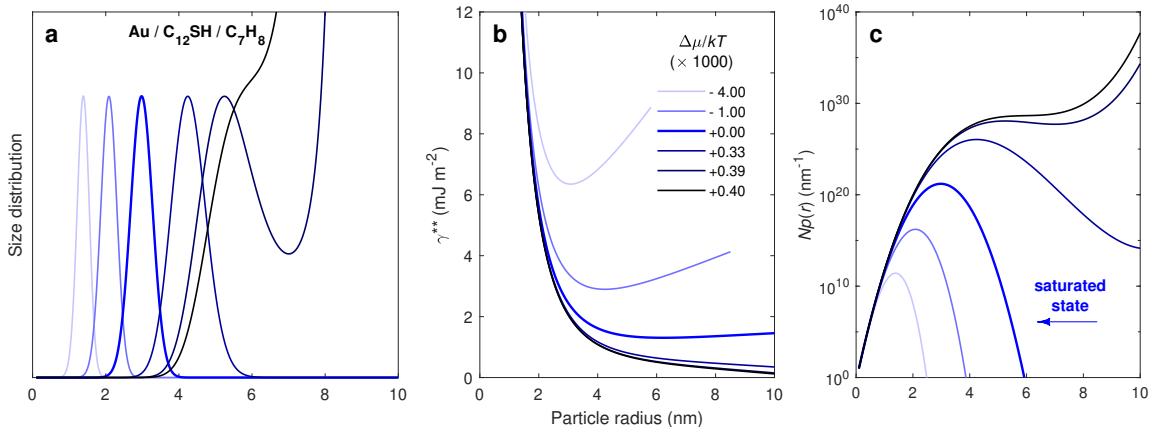


Figure 3. Modification of the size distribution of hypothetical gold-thiol colloids by changing the chemical potential of monomer relative to the bulk phase according to Eq. 21. The state of equilibrium between monomer, colloid, and bulk ($\Delta\mu = 0$) is given by the thick blue line (arrow in (a)). Paler colors indicate increasing degrees of undersaturation; darker colors indicate increasing supersaturation. (a) Size distributions scaled to show differences in mean radius and distribution shape. (b) the corresponding effective interfacial free energy densities γ^{**} , including the “size-dependent” contribution from $\Delta\mu$. (c) Logarithmic plot of the particle concentrations (not necessarily corresponding to physically possible conditions: see Figure S2).

by the retention of peaks in the distribution in Figure 1a for $1000\Delta\mu/kT = +0.33$ and $+0.39$. For sufficiently large $\Delta\mu$ ($+0.4$ curve in Figure 1a), the $\exp n\Delta\mu/kT$ term dominates the “size distribution.” The point at which the size distribution is no longer peaked, i.e. becomes monotonically increasing, can also be taken as an indication of the system’s instability to homogeneous nucleation and growth. As $\Delta\mu$ increases, the “mean” particle radius at the peak in the distribution increases accordingly, along with the particle concentration (Figure 3c), although the situation in Figure 3 is not necessarily physical. The volume fraction of Au calculated from the (truncated) integral of $Np(r)$ exceeds the upper limit of what might be called reasonable values ($\phi = 0.1$) for rather small values of $\Delta\mu$, as illustrated in Figure S2a in the Supporting Information. (In fact, even the curve for the least supersaturated solution in Figure 3, $1000\Delta\mu/kT = +0.33$, does not correspond to a physically reasonable situation.) Although the model demonstrates it should be possible from this model to “tune” the average particle size through dilution or concentration of the colloidal solution—albeit requiring changes in concentration over many orders of magnitude—from an engineering perspective this remains unexplored.

It is clear from Figures 3a and 3c that the shape of the distribution does not change markedly while $\Delta\mu$ is not too positive. The polydispersity, indeed, is practically independent of the degree of saturation: Figure S2b shows that, over a range of ten orders of magnitude in particle concentration, the polydispersity only varies from 10% (its starting value) to less than 11%. The weak dependence of polydispersity on $\Delta\mu$ can be understood qualitatively in view of the fact that, following from Figure 2, the width of the particle size distribution closely follows the *curvature* of the $r-\gamma^{**}$ relationship. Since the $\Delta\mu$ term in γ^{**} goes as r^1 , it does not contribute to $d^2\gamma^{**}/dr^2$. Although we mentioned in the previous section that the size distribution can be made very narrow if both $\gamma^* < 0$ and $\Delta\mu < 0$, this case does not occur for the experimental systems we subject to analysis in Section 3. Thus, engineering of particle size distributions probably must be made by the choice of mechanism through which the excess interface energy changes, rather than by controlling concentrations of reagents.

3.1 Experimental interpretation

We also test the statistical thermodynamic approach to nanoparticle size distributions summarized in Eq. 12 against experimental data. Nanoparticle size data has been almost universally reported in terms of a histogram giving the number of particles having a size falling in a particular bin, the measurements being

obtained by means of TEM or other microscopy techniques. This consists of a set of L bins evenly spaced by 2ℓ , with the i th bin having bin center r_i and number of counts c_i . For both retro- and prospective analysis of such size distributions, we now describe a method for estimating $Np(r)$ from such a histogram as our means of analyzing older experimental data. Briefly, from a value of the volume fraction of solid ϕ surmised from the experimental procedure, we obtain an estimate for the total number of colloidal particles N in the solution based on the histogram according to

$$N = \frac{3\phi}{4\pi \langle r^3 \rangle},$$

where the mean cubed radius $\langle r^3 \rangle$ is estimated by

$$\langle r^3 \rangle = \frac{\sum_i r_i c_i}{\sum_i c_i}.$$

We then approximate $p(r)$ as a piecewise continuous uniform distribution. Within each bin,

$$p(r_i) \approx \frac{c_i}{\sum_i c_i} \frac{1}{2\ell},$$

which is our estimate of $Np(r)$ at the bin center. Where n is sufficiently large that it can be treated as a continuous variable (a reasonable approximation for the large values of n for particles of radius in the nm range), the size distribution in terms of r , following Eq. 12, is

$$Np(r) = 4\pi r^2 \rho_b q_n^{(ext)} e^{\frac{4\pi r^3 \rho_b}{3kT} \Delta\mu} e^{-\frac{4\pi r^2 \gamma^*}{kT}} \quad (29)$$

where n in $q_n^{(ext)}$ depends implicitly on r . The exponent of r in $r^2 q_n^{(ext)}$ derived from Eqs. 15–19 is thus $3\beta + 2$ where β was the original exponent of n . (The Lothe-Pound⁴⁹ case is notable in this regard, since $3\beta + 2 = 14$, which was the exponent for r noted by Volmer in 1956.⁸⁸) The estimate for the size-dependent interfacial free energy is

$$\gamma^{**}(r) = -\frac{kT}{4\pi r^2} \ln \frac{4\pi r^2 \rho_b q_n^{(ext)}}{Np(r)}. \quad (30)$$

More details on the fitting procedure, and the experiments examined here, are available in Sections S7–S8 of the Supporting Information. Our task then is to fit Eq. 29 or Eq. 30 having at most four undetermined parameters to, at minimum, an experimentally known size distribution and solid concentration. Ideally, an experiment would determine the function N_n for each directly measurable n , as in a mass spectrometric measurement, or the continuous version of $Np(r)$. Size distributions are much more frequently reported, especially for nanoparticles, as combining a set of dimensional measurements made from microscopy images. The r measurement so obtained is that of the high-contrast inorganic core, which we use here exclusively. (Different techniques, such as mass spectrometry, will return a size distribution that includes the surfactant shell, and thus a slightly different polydispersity.)

Virtually all work on nanoparticle syntheses to date by methods of (ostensibly) thermodynamic stabilization have quantified the particle size distribution in terms of only two parameters, the number average diameter and the standard deviation of the diameter about the mean. A frequent assumption for nanoparticle sizing in general is that relatively monodisperse size distributions follow a simple normal or log-normal distribution, both of which have only two arguments in $p(r)$. However, in a quantitative estimate of γ , it is necessary also to know the absolute concentration of solid matter in the colloidal solution, which adds a third parameter to the size distribution. We can use these three-parameter normal or lognormal functions as a benchmark against the physically-motivated expressions for the size distribution embodied by Eq. 12.

3.2 Fitting of experimental data

We consider data from two previously reported investigations in colloidal nanoparticle systems that are proposed to be thermodynamically stable. First, Stoeva et al.²⁰ gave an example from the frequently-investigated class of nanoparticle syntheses known as digestive ripening, in which large metal nanoparticles

are heated with an excess of surfactant in organic solvent, breaking apart into smaller particles with a narrow size distribution. In their case gold (Au) nanoparticles were digested in toluene (C_7H_8) with dodecanethiol ligand (called here $C_{12}SH$), with a molar ratio of dodecanethiol to Au of 30:1. The resulting colloids had a radius (r) of $\approx 2.3 \pm 0.2$ nm (the latter quantity being one sample standard deviation) and volume fraction of $\phi \approx 1.3 \times 10^{-4}$. Second, Vayssières^{21, 22} suggested that magnetite (Fe_3O_4) nanoparticles in highly basic (pH 12), high-ionic-strength (0.5 M) aqueous solutions adopted a thermodynamically stable size distribution due to the enthalpies of adsorption of hydroxyl ions (OH^-) and electrical double layer formation. In this case, $\langle r \rangle \approx 3.3 \pm 0.8$ nm and $\phi \approx 4.0 \times 10^{-3}$. In Section S8 of the Supporting Information we reproduce the estimates of the number of counts in each bin in Tables S3 and S4, along with particulars of how they and ϕ were determined.

In analyzing this data we have made several assumptions we feel are reasonable. First, we expect that the values of ϕ we have mentioned follow directly from the input mass or concentration of solid monomer (Au atoms or Fe ions, respectively) and have been entirely converted to solid nanoparticles with negligible dissolved monomer. In the case of magnetite, which is believed to dissolve as iron hydroxides $Fe(OH)_x$, the solubility of the bulk phase has been measured and found to be extremely low (less than 1 μM) in basic media.⁸⁹ Thiol surfactants are known to corrode Au in specific environments, but in toluene the molecular solubility (likely as an Au thiolate polymer or other compound) has been reported to be minimal.⁹⁰ Although with these assumptions we can disregard the identity of the monomer(s) and surfactants entirely, abstracting their chemical potentials into γ^* and $\Delta\mu$, being able to provide estimates of their magnitude will be critical to future models of the adsorption energies and the phase equilibrium in the system; without them it is, for example, unknown at what temperatures spontaneous precipitation, dispersion, or dissolution will occur.

Second, we have assumed that bulk values of the formula unit density were applicable for nanoparticles (both for solids and surfactants) and neglected temperature dependence of these parameters (except for the solvents, because tabulated values were readily available, but this is unlikely to make any difference). Third, we included the volume and mass of $C_{12}SH$ surfactant molecules in calculating $q_n^{(ext)}$ for the Au/ $C_{12}SH$ system (estimates of surfactant densities are available for Au surfaces and nanoparticles^{91, 92}), but calculated $q_n^{(ext)}$ based solely on the mass and radius of a Fe_3O_4 sphere for the $Fe_3O_4/OH^-/H_2O$ system because we could not arrive at a conclusion as to how the adsorbed hydroxide “surfactant” shell, together with the electrical double layer, should be represented in $q_n^{(ext)}$. Finally, the surfactant grafting density in the former case was assumed to be independent of curvature. The reference values used the Au/ $C_{12}SH$ and Fe_3O_4/OH^- systems are given in the Supporting Information.

In a given fit, one of $q_n^{(LP)}$, $q_n^{(RKC)}$, or $q_n^{(K)}$ is inserted into Eq. 11 along with Eq. 27, possibly with one or more values restricted. We found it was sometimes not immediately obvious which model produces the better fit or whether the fit was improved by using a full four parameters instead of three. It is necessary, then, to use some kind of criterion to evaluate the usefulness of adding an extra fitting parameter and to compare the goodness of fit using the physically motivated Eq. 12 to the qualitative normal or lognormal distributions. For this we use the reduced chi-square test according to the χ^2 statistic,⁹³ as described in Section S9 of the Supporting Information. Between two fits, the one with the smaller value of χ^2 is the better one. The values of χ^2 for these fits are given in Tables 1 and 2. Because the number of counts for large r in both datasets is so small, we did test some fits with the size distribution truncated to removed the rightmost two bins (having one or two counts each), but found no real effect on the magnitude and standard error of the relevant parameters (not shown). We stress here that future experiments wishing to use this analysis should greatly increase the number of samples taken to mitigate overfitting of the data, or else use ensemble techniques: here we are forced to use three or four parameters, plus a choice of $q_n^{(ext)}$, to fit only 9-12 data points.

Table 1: Goodness-of-fit $\tilde{\chi}^2$ values for each combination of $q_n^{(ext)}$ and γ^{**} for Ref. 20, figure 6.

Model	$q_{ext}^{(LP)}$	$q_{ext}^{(RKC)}$	$q_{ext}^{(K)}$
$ar^b + \delta r + \gamma_0$	0.0725	0.0815	0.0746
$ar^b + \gamma_0$	0.1028	0.0780	0.0973
$ar^{-3} + \delta r + \gamma_0$	0.0742	0.1294	0.0914
Normal	0.1413		
Lognormal	0.0720		

Table 2: Goodness-of-fit $\tilde{\chi}^2$ values for combinations of $q_n^{(ext)}$ and γ^{**} for Ref. 21, figure 11d.

Model	$q_{ext}^{(LP)}$	$q_{ext}^{(RKC)}$	$q_{ext}^{(K)}$
$ar^b + \delta r + \gamma_0$	0.0115	0.0102	0.0112
$ar^b + \gamma_0$	0.3570	0.3431	0.3623
$ar^{-2} + \delta r + \gamma_0$	0.0424	0.5568	0.3517
Normal	0.4676		
Lognormal	0.0654		

3.3 Fitting results

A summary of the results of fitting the expression of Eq. 12 are shown in Figure 4. Superimposed in Figures 4a-b are the extracted piecewise uniform distribution functions (the experimental histograms, shaded area) and the $p(r)$ obtained by dividing the fitted $Np(r)$ expression by the N estimated from the histogram (full lines). The error bars have been drawn assuming Poisson statistics, i.e., for a value of $p(r)$ at a size r_i , $p(r_i)$, the estimated standard error is $p(r_i) / \sqrt{c_i}$ where c_i is the number of counts in the bin. The choice of $q_n^{(ext)}$ does not meaningfully affect the fit when all four parameters of γ^{**} are free—the fitted size distributions will overlap almost perfectly. The excess interfacial free energy densities of each system, as calculated using $q_n^{(LP)}$ and the form of γ^{**} for the fits in Figure 4a-b, are shown in Figure 4c.

The values of the parameters from the fits and their uncertainties for the models of γ^{**} are given in Tables 3–4. It is plain from Figure 4a–b that the fits to $Np(r)$, where all four of a , b , δ , and γ_0 are free, are quite good. Also in evidence is a skew of both distributions to larger particle sizes: fits to a normal distribution are poor compared to the physically motivated form of Eq. 12 or a lognormal distribution, as shown by Figure S3 in the Supporting Information. For the Au/C₁₂SH system, a lognormal distribution describes the data as well or better than Eq. 12, as measured by $\tilde{\chi}^2$, but this distribution shape still falls short for the Fe₃O₄/OH[−] system, which is too right-skewed. When particle size distributions become less polydisperse, as for the former system, better counting statistics and narrower bins will necessary to distinguish between different analytical forms used to fit them. Inspection of Tables 3–4 shows that the lowest $\tilde{\chi}^2$ values are found using $q_{ext}^{(LP)}$ and $q_{ext}^{(RKC)}$ for the Au/C₁₂SH and Fe₃O₄/OH[−] systems, respectively, but the differences in $\tilde{\chi}^2$ values between models are not very large. We feel, in fact, that the differences are too small to prefer strongly one form of $q_n^{(ext)}$ over another based on these criteria alone. More detailed reporting of experimental data would help here. For example, a list of measured sizes instead of binned histograms would improve confidence in statistical tests. In general, future data sets will need to make more than a few hundred measurements; this number was otherwise suitable for reports of syntheses intending to give only estimates of the mean and standard deviation.

The model of Eq. 12 is flexible enough to accomodate any choice of $q_n^{(ext)}$ for both systems as measured by the $\tilde{\chi}^2$ metric, such that additional curves in Figure 4a-b would be practically indistinguishable from that already plotted. Interestingly, for most choices of $q_n^{(ext)}$, the value of b was non-integral with the nearest integer lying well outside the standard error of the parameter estimate. In the Au/C₁₂SH system the exponents covered a wide range from about -3.2 for $q_n^{(LP)}$ to -4.5 for $q_n^{(RKC)}$. On the other hand, b in the

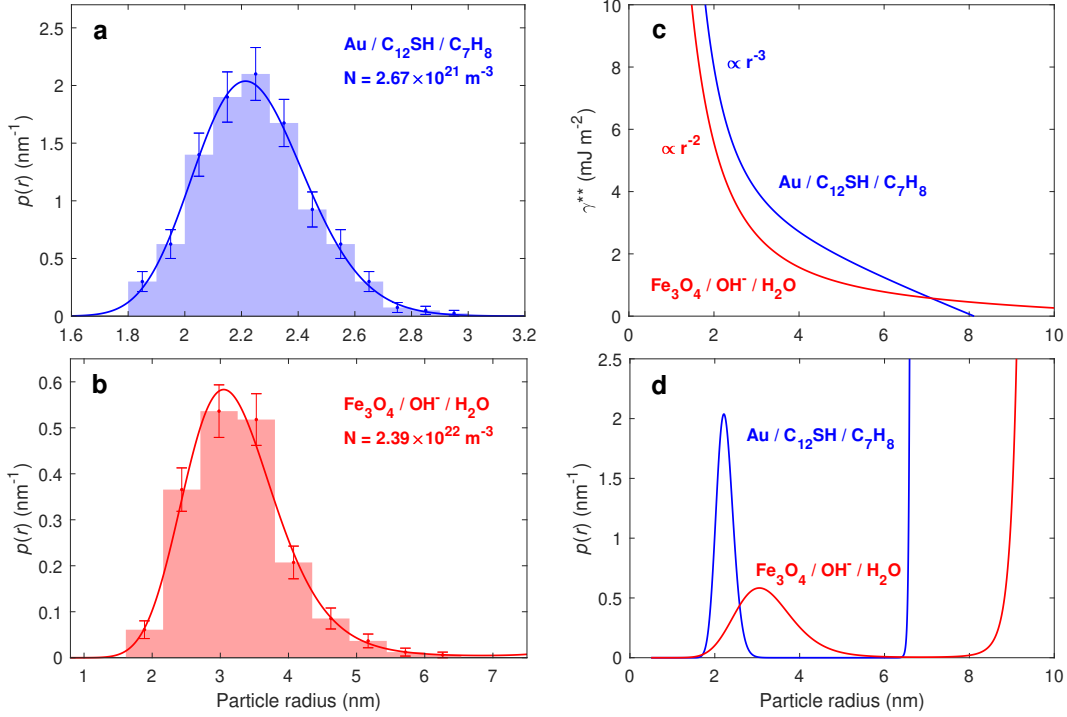


Figure 4. Application of Eq. 29 to experimental data. The Au/C₁₂SH/C₇H₈ data were extracted from Ref. 20; the Fe₃O₄/OH⁻/H₂O data, from Ref. 21. (a,b) The fitted particle size distributions according to a power-law dependence of γ^{**} on radius (b) The estimated size-dependent interfacial free energies. The approximate size dependence for small radii is indicated by the exponent of the radius next to each curve: the exponents of r are, for Au/C₁₂SH/C₇H₈, close to -3 (that for the electrostatic charging model) and, for Fe₃O₄/OH⁻/H₂O, almost exactly -2 (that for the Helfrich model for Gaussian curvature bending energy). (d) the estimated probability density functions for the size distributions based on (a); note that the distributions diverge for larger particle radii.

Fe₃O₄/OH⁻ system occupied a much more restricted range: about -2 through -2.4 . though we presently cannot offer suggestions as to how such an exponent, which might better be described as reflecting a more complex dependence of γ^* on r , would arise. As noted for Figure 2, the smaller range of radii enclosed by the less polydisperse (10%) Au/C₁₂SH data set here (relative to Fe₃O₄/OH⁻, polydispersity of about 20%) correspondingly reduces the span of γ^{**} , with the result that for similar estimated errors in particle concentrations in each bin the data will be more easily fit by a wide range of exponents. Different mechanisms for the size dependence of γ^* appear to operate depending on the environment and solid material chosen for the colloid, and it is plausible that these mechanisms may follow rules more complex than the power law in Eq. 27.

Table 3: Extracted fit parameters for Ref. 20, figure 6 using the four-parameter form of γ^{**} .

Parameter	$q_{ext}^{(LP)}$	$q_{ext}^{(RKC)}$	$q_{ext}^{(K)}$
a (J nm ^{-2-b})	0.0422(1)	0.0351(2)	0.0383(1)
b	-3.16(1)	-4.47(1)	-3.45(1)
δ (J nm ⁻³)	-0.000548(9)	-0.000135(4)	-0.000432(7)
γ_0 (J m ⁻²)	0.00436(4)	0.00187(1)	0.00363(3)

Table 4: Extracted fit parameters for Ref. 21, figure 11d using the four-parameter form of γ^{**} .

Parameter	$q_{ext}^{(LP)}$	$q_{ext}^{(RKC)}$	$q_{ext}^{(K)}$
a (J nm $^{-2-b}$)	0.02071(4)	0.01032(5)	0.01849(4)
b	-1.997(4)	-2.341(8)	-2.058(4)
δ (J nm $^{-3}$)	-0.0000249(8)	-0.0000216(5)	-0.0000249(7)
γ_0 (J m $^{-2}$)	0.000333(7)	0.000290(5)	0.000332(7)

In general, good fits of the size distribution expression to the data of Figure 4a-b could only be achieved with a value of δ that was negative, that is, where $\Delta\mu > 0$. This corresponds to a situation in which the solution is supersaturated with monomer and where the nanoparticle size distribution is, in fact, metastable or unstable. The curves in Figure 4d illustrate this tendency: at radii several nm larger than the mean, the “size distributions” diverge. In the case of the Au/C₁₂SH system, it is uncertain whether the fit is significantly improved by the addition of this parameter δ . The best fits overall are achieved using $\delta \neq 0$, but the values of χ^2 depend markedly on the choice of $q_n^{(ext)}$, such that the three-parameter model with $\delta = 0$ can achieve goodness-of-fit close to that of the four-parameter model. We therefore deem it ambiguous from the point of view of Eq. 12 whether $\Delta\mu > 0$ in this system, but note that previous work showed that prolonged treatment of these colloids produced by digestive ripening at high temperatures led to their coarsening.⁹⁴ It would seem then that, if the Au/C₁₂SH system is really stable ($\Delta\mu \geq 0$) at lower temperatures, it must be close to instability.

The sign of $\Delta\mu$ was far less ambiguous in fitting the data for the Fe₃O₄/OH⁻ system, which is also visually more fat-tailed at large r . If b were fixed at -2 , only $q_n^{(LP)}$ with $\delta < 0$, or the full four-parameter model, produced a good fit to the data. If γ^* in this case follows a power law, the fat tail of the size distribution cannot be well-fit unless $\delta < 0$, as clearly shown by Table 2. That the Fe₃O₄/OH⁻ system is more restrictive in terms of its fit to theory follows from the fact that, relative to the Au/C₁₂SH system, the size distribution of Figure 4b spans a larger range of particle radii (2–6.5 nm, versus 1.75–2.75 nm). Hence, the curvature of γ^* that follows from the power law is more tightly constrained. Vayssières noted that, in bringing a Fe₃O₄ colloid from a region of thermodynamic instability to one of ostensible stability, although a population of smaller nanoparticles was formed from a coarser dispersion, in line with the expectations of a thermodynamically stable nanometric size, very large particles remained even after 30 days, leaving a bidisperse distribution. They attributed this observation to the very slow kinetics of dissolution and re-precipitation of nearly insoluble oxides, but it is equally well-explained if, in the initial preparation conditions, $\Delta\mu$ began at a value less than 0, so that bulk Fe₃O₄ would precipitate until an equilibrium between the bulk phase and colloidal solution was achieved, with $\Delta\mu = 0$. Another possibility is that the experimental time scale was too short to allow N to change significantly, in which case the equilibrium condition of Eq. 12 does not apply. In fact, the model laid out by Lee et al.³², which does work at fixed N , would account for such a bidisperse distribution. Ultimately, we strongly suspect that, under the reported experimental conditions, this Fe₃O₄/OH⁻ system does not represent a true thermodynamic minimum with respect to N , but is only metastable.

We additionally fitted the size distributions using 1) a fixed value of b or 2) a fixed value of $\delta = 0$ in Eq. 27. The restriction of parameters tests the utility of more parsimonious (nested) models. In the first case the known value for b corresponded to a specific mechanism of size-dependent γ : -3 for the Au/C₁₂SH/C₇H₈ system, per the electrostatic charging model discussed by Lee et al.³² and Manzanares et al.; and, for the Fe₃O₄/OH⁻/H₂O system, -2 per the Helfrich model of Gaussian curvature energy⁹⁵ also considered by Whetten and Gelbart for the Au/C₁₂SH system.⁸⁵ These values were suggested by the values of b from the full four-parameter fits. Despite the increase in the number of degrees of freedom, the goodness of fit statistic was either unimproved or slightly worsened. Interestingly, however, $b = -3$ accounted for the data in Figure 4a just as well as any of the $q_n^{(ext)}$ models in the more flexible four-parameter fit. At the current resolution of this data, the model of electrostatic charging of nanoparticles in a dielectric medium provides a good accounting for the data from the digestive ripening of gold nanoparticles provided the saturation parameter $\Delta\mu$ —which is not at any rate currently known—is adjustable.

Conversion of the resulting values of a , δ , and γ_0 to the underlying physical parameters provided entirely reasonable results (fit details also in Section S8.1–S8.2 of the Supporting Information). For Au/C₁₂SH,

the corresponding number of elementary charges per nanoparticle was about 3, similar to the value of 5 assumed by previous workers.^{32, 41} The value of the curvature or saddle-splay modulus, $\bar{\kappa}$, for the $\text{Fe}_3\text{O}_4/\text{OH}^-$ system is about 2×10^{-20} J, which is about an order of magnitude lower than the typical bending energy of an organic monolayer.^{95, 42} Of course, there is no such surfactant monolayer in this system—only adsorbed anions surrounded by an electrical double-layer—so a better explanation for such an r^{-2} dependence of γ for this aqueous system is probably needed. From the term δ in γ^* , the interfacial free energy densities at zero curvature are estimated to be 3.7 mJ m^{-2} and 0.38 mJ m^{-2} for the the $\text{Au}/\text{C}_{12}\text{SH}$ and $\text{Fe}_3\text{O}_4/\text{OH}^-$ systems, respectively. The positive sign of γ_0 for the former system is interesting in the context of prior models of the Au-thiol system, where the binding energy of thiol per area was generally taken to be so large (negative) compared to the surface energy of a clean Au surface that the effective interfacial energy, $\gamma^* = \gamma + \epsilon^* (\mu_s - \mu_s^*)$, was *negative* at large radii. In these models the convergence of the size distribution in Eq. 12 is assured by having the solution be undersaturated in monomer with respect to the bulk, i.e. a negative $\Delta\mu$. Instead, we have shown here for these systems γ_0 remains small and positive, and mean nanoparticle size is inversely proportional to the magnitude of the interfacial free energy as in the case of microemulsions⁶⁸ or in earlier models of the spontaneous dispersion of solids.^{96, 37} We note as well that the value of γ_0 for the $\text{Au}/\text{C}_{12}\text{SH}$ system is of similar magnitude to solid-liquid interfacial free energies measured for some small organic molecules,⁹⁷ which makes some sense considering that the interfacial free energy of a saturated Au-thiol monolayer should reflect the interactions between the organic solvent (here, toluene) and the ends of the surfactant molecules (here, dodecanethiol), rather than the inorganic nanoparticle core. This suggests a potential avenue for engineering the properties of the size distribution by selecting molecular characteristics of the surfactant that control the flat-surface limit of the solid-solution free energy, in addition to the mechanism through which a power-law dependence of γ^* appears.

3.4 Further consequences of the size distribution-interfacial energy correspondence: Future avenues for quantifying system parameters

Quantitatively fitting experimental size distributions at a fixed temperature, pressure, concentration, and so on is only one part of the characterization of the ternary solid-surfactant-solvent system. To close, we give here elaborations on Eq. 12 that can be used to measure quantities like colloid-surfactant stoichiometry and the exponent β from $q_n^{(ext)}$ when future work permits the analysis of more complete data sets on particle size distributions. Because the experimental data considered here are sparse, in that the dependence of the size distribution on experimental variables for colloidal nanoparticles has not been adequately explored, we cannot apply any of the analysis in this section to that data and leave such for future work on these systems. Considering the expression for the chemical potential of component i , $\mu_i = \mu_i^0 + kT \ln a_i$, if we rewrite Eq. 7 as

$$\begin{aligned} N_n &= q_n^{(ext)} \exp \left[\frac{n (\mu_1^0 + kT \ln a_1) - n (\mu_b^0 + kT \ln a_b) - (n\epsilon - \epsilon_n) (\mu_s^0 + kT \ln a_s)}{kT} \right] \\ &\times \exp \left[\frac{\epsilon_n (\mu_s^{*0} + kT \ln a_s^*) - 4\pi r^2 \gamma}{kT} \right] \\ &= q_n^{(ext)} \frac{a_1^n}{a_b^n a_s^{n\epsilon}} (a_s a_s^*)^{\epsilon_n} \exp \left[\frac{n\mu_1^0 - n\mu_b^0 - (n\epsilon - \epsilon_n) \mu_s^0 + \epsilon_n \mu_s^{*0}}{kT} \right] \exp \left[-\frac{4\pi r^2 \gamma}{kT} \right], \end{aligned}$$

the quotient $a_1^n/a_b^n a_s^{n\epsilon}$ is recognizable as the experimentally measurable monomeric solubility product, K_{sp} . Since activities of condensed phases are unity, $K_{sp} = a_1^n/a_s^{n\epsilon}$. Differentiating $\ln N_n$ with respect to a quantity ω other than n gives

$$\frac{d \ln N_n}{d\omega} = \frac{d}{d\omega} \left[\ln q_n^{(ext)} + \ln K_{sp} (a_s^* a_s)^{\epsilon_n} - \frac{4\pi r^2 \gamma}{kT} \right].$$

The most natural experimental parameters to vary are the concentrations of surfactant and the temperature. For the former, assuming small changes in the composition of the solution phase do not affect γ or ϵ_n , and

thus a_s^* ,

$$\frac{d \ln N_n}{dN_s} = \frac{d\epsilon_n \ln a_s}{dN_s},$$

and taking $a_s = b_s X_s$ where b_s is the activity coefficient of the surfactant and X_s is its mole fraction $N_s/(N_s + N_l)$ (likely to be practically unaffected by N_n due to the small volume fraction of colloidal solid), we obtain

$$\frac{d \ln N_n}{dN_s} = \epsilon_n \left(\frac{1}{N_s} - \frac{1}{N_s + N_l} \right). \quad (31)$$

This gives the surfactant coverage density, possibly size-dependent, as a function of the concentration of surfactant.

In the case of temperature, for small changes that do not appreciably affect the concentration of unbound surfactant (reflected in a_s) or the stoichiometry of the surfactant shell (reflected in a_s^*),

$$\frac{d \ln N_n}{dT} = \frac{d \ln q_n^{(ext)}}{dT} + \frac{d \ln K_{sp}}{dT} + \frac{4\pi r^2 \gamma}{kT^2}.$$

Because by definition $\ln K_{sp} = -(\Delta h_{sp} - T\Delta s_{sp})/kT$ where Δh_{sp} and Δs_{sp} are the enthalpies and entropies of the monomeric solubility equilibrium, we finally obtain (assuming those energetic parameters are constant with T)

$$\frac{d \ln N_n}{dT} = \frac{d \ln q_n^{(ext)}}{dT} + \frac{4\pi r^2 \gamma - \Delta h_{sp}}{k} \frac{1}{T^2}. \quad (32)$$

Deviations of $d \ln N_n/dT$ from linearity in $1/T^2$ arising from $q_n^{(ext)}$ are to be expected, and provide a probe of the size-dependent statistical thermodynamic properties associated with the motion of the nanoparticles in the solvent.

Provided the appropriate experimental conditions are met, the limiting forms of the size distribution with respect to r provide valuable information from the tails of the distribution. The logarithm of Eq. 12 indicates a natural manner of graphically determining physicochemical parameters of the system,

$$\begin{aligned} \ln N_n &= \ln \alpha r^\beta - \frac{4\pi r^2}{kT} (ar^{-b} + \delta r + \gamma_0) \\ \ln N_n - \ln \alpha &= \beta \ln r - \frac{4\pi a}{kT} r^{2-b} - \frac{4\pi}{kT} (\delta r^3 + \gamma_0 r^2) \end{aligned} \quad (33)$$

In cases where b can be assured to be 2 by the appropriate choice of system, for small r the ar^{-b} term predominates and

$$\ln N_n + \frac{4\pi a}{kT} - \ln \alpha = \beta \ln r. \quad (34)$$

That is, the slope Y of $\ln N_n$ versus $\ln r$ provides, for small r , a measurement of the entropic quantity β . If αr^β is assumed or known, taking the logarithm of 33 again yields

$$\ln \ln \frac{\alpha r^\beta}{N_n} = \ln \left[\frac{4\pi}{kT} (ar^{2-b} + \delta r^3 + \gamma_0 r^2) \right]. \quad (35)$$

If $B \geq 2$, then for large r the ar^{-b} term disappears, and the plot of $\ln \ln \alpha r^\beta / N_n$ versus $\ln r$ at large r will have slope 2 and intercept of $\ln 4\pi/DkT$ if $\delta = 0$ (colloidal solution at equilibrium with bulk solid), or slope 3 and intercept $\ln 4\pi\delta/kT$ if $\delta > 0$ and $\gamma_0 < 0$ (solution undersaturated relative to bulk, but with a negative interfacial free energy). Conversely, for small r , the slope will approach $2 - b$ and the intercept $\ln 4\pi a/kT$.

Because the tails of the distribution necessarily have exponentially worse counting statistics, however, it is unclear how achievable it is to obtain good data for which the approximations $r \rightarrow 0$ or $r \rightarrow \infty$ are valid,

especially in a microscopy experiment. For example, the limit of small r implies an approach to molecular dimensions where the capillarity approximation required by Eq. 9 is invalid. For example with regards to Eq. 34, in fitting the data of Vayssières (discussed in more detail in Section 3.4) with $q_{ext}^{(LP)}$ (Eq. 15) to a γ of $ar^{-2} + \gamma_0$, at $r = 1$ nm, $d \ln N_n / d \ln r$ is still only about 12.5, rather than 14, and this particle size lies almost four standard deviations from the mean radius of the data set. Using $q_{ext}^{(RKC)}$ (Eq. 18) instead, the slope at $r = 1$ nm is about 4.2 as opposed to 3.5. In fact, estimating β from those experimental data here is impossible, since there are no data points in this size range and the bin width is prohibitively large. If $q_n^{(ext)}$ cannot actually be written in the form ar^β , as is true when, e.g., surfactant molecules contribute to the mass and moment of inertia of the colloid in $q_n^{(LP)}$, the plot from Eq. 34 also will not be linear. Hence, although Eqs. 34 and 35 are measurements of the statistical mechanical basis of CNT as well as the physicochemical parameters of the system, it will be difficult in future experiments to assure reasonable statistics, since the necessary data comes from in a size range lying outside of nearly all samples that could be drawn from the underlying distribution. Still, should these difficulties be overcome, combining the expressions given in this section with the fitting of the distribution to Eq. 12 will provide a wealth of information on the thermodynamics of the solid-solution interface in colloids.

4 Conclusions

In spite of the frequent assumption that nanometric colloids of solids are intrinsically thermodynamically unstable (lyophobic), due to the tendency to minimize interfacial free energy, phenomenological and statistical thermodynamic treatments show this is not necessarily the case. Classical nucleation theory (CNT) provides the statistical thermodynamic basis for calculating the size distribution of colloids at equilibrium based on physically motivated or measurable parameters. We examined previous statistical-mechanical models of the work of cluster formation which provide different, and contested, accountings of the total degrees of freedom of an aggregate or colloidal particle separated from the bulk and allowed to move in a different medium. These give rise to different dependences of the colloid concentration on particle size based purely on entropic considerations, manifesting as a different prefactors and polynomial exponents alongside the reversible work of nanoparticle formation from the bulk phase. We also provided a simple, intuitive extension of the cell model of liquid mixtures to describe the external partition function in terms of vibrational frequencies that can be estimated theoretically. Based on these models, an exact relation exists between the excess free energy per particle normalized by the interfacial area and the observed particle concentrations of all sizes.

For a narrow distribution of relatively large (nm-sized) particles to exist, γ must be a function of radius purely on statistical-mechanical grounds. The absolute value of γ depends rather markedly on the model used for the external and internal degrees of freedom, especially on the fixed prefactor rather than the n -dependent polynomial term. Inspection of simulated distribution shapes shows that, owing to the exponential dependence of particle concentration on γ , the range of values of r for which γ can be estimated from experiments such as particle counting may be restricted when using measurement techniques that rely on counting particle sizes manually via microscopy. Even within the applicable range of particle sizes, great care needs to be taken in experiments to minimize uncertainty in r , as in binned measurements. A well-executed ensemble measurement, though, could measure the size-dependent thermodynamics of the system over a wide range of particle sizes. Next, from an engineering perspective, factors such as under- or supersaturation, i.e. controlling the dilution of the solution, as well as the zero-curvature interfacial free energy, are probably not the principal contributors to the polydispersity of the colloid. The minimum achievable polydispersity is mechanism-dependent and is proportional to the curvature of γ in the vicinity of the distribution mean: interfacial free energy densities that increase more rapidly with increasing interface curvature will lead to narrower size distributions. This stands in contrast to kinetically controlled synthetic approaches that have primarily focused on controlling the non-equilibrium supersaturation during particle nucleation and growth.

On a more empirical level, we adapted CNT to the fitting of experimentally reported size distributions in both an organic and an aqueous solvent system. The first corresponded to a typical experimental case in the relatively well-studied systems of digestive ripening of metals by strongly bonding surfactants,²⁰ while the second corresponded to a high-ionic-strength, high-pH oxide dispersion.²¹ CNT was used to analyze these models by use of the physically motivated power-law dependence of γ on particle size as a fitting parameter. The resulting effective interfacial free energy γ^{**} depends on this mechanism-specific power law, the under-

or supersaturation of monomer with respect to the bulk, and the interfacial free energy density in the limit of flat interfaces. Fits of the experimental data based on the analytical size distribution, Eq. 12, proved to be excellent; the best fits could, interestingly, be made with a non-integer exponent of the particle curvature. A non-integer exponent is not anticipated by simpler expressions for the excess interfacial energy based on, e.g., capacitive charging or curvature moduli, and could indicate that a more complex model is needed to explain the size dependence of the interfacial free energy. Still, in the gold-thiol-toluene system, the data could still be well-modeled by the hypothesis that the energy of electrostatic charging of the metal colloid in a dielectric medium, which is related to particle radius as r^{-3} , accounts for the excess interfacial free energy. In fitting, a fat tail at large particle sizes in the distributions strongly supports the hypothesis that the solution is supersaturated, having monomer at a higher chemical potential than the bulk solid. This is in contradiction to some previous thermodynamic modeling that required undersaturation of the solution to assure the stability of the colloid. We suggest that although the two systems analyzed here are apparently resistant to precipitation as a bulk solid, they nonetheless have only so far been observed in a *metastable state*. This would account for the apparent failure to observe a bulk-to-colloid dispersion process in systems such as digestive ripening.²⁰ Before proceeding any further with size-distribution analysis, future workers should decisively test whether these systems really occupy the global minimum of free energy relative to the molecular solution and bulk phases. Given the low precision associated with measurements of distribution tails due to counting statistics, it is clear better statistical tests and especially finer-grained size distribution measurements are desired to distinguish between competing models or expressions, especially with regards to the supersaturation parameter. This must also be done to avoid the problem of overfitting, as so far these data sets require fitting only 9-12 data points with four parameters. Finally, we have shown here several relations between the size distribution and the external parameters of the system (surfactant concentration, temperature) that will be useful for measuring interfacial properties over a broader composition space or for checking the validity of our approximations. Limiting forms of the size distribution show that the tails of those distributions, which have generally not been subjected to scrutiny due to the difficulty in obtaining good measurement statistics far from the mean, could provide a way to directly measure the parameters linked with the CNT description of the entropy of these large, rigid molecules in solution. The size distribution–interfacial energy correspondence could thus provide a new method for testing statistical thermodynamic models or simulations for macromolecular solutions and other mixtures of molecules of very different sizes.

Supporting Information

Sections S1–S9: material-specific values used in calculations, details of calculations of excess properties and size distribution parameters, supplementary plots to Figure 3, estimated data sets from References 20 and 21, and additional notes on the fit results with supplementary plots for Figure 4.

Acknowledgments

A.N. is supported by the National Academies of Science, Engineering, and Medicine via an NRC Postdoctoral Research Associateship. We thank John Pettibone (NIST, Materials Measurement Science Division) and James Hickman and Yuri Mishin (NIST, Materials Science and Engineering Division) for helpful discussions.

Certain commercial equipment, instruments, and software are identified in this paper in order to specify the experimental procedure adequately. Such identification is not intended to imply recommendation or endorsement by the National Institute of Standards and Technology, nor is it intended to imply that the equipment or software identified is necessarily best available for the purpose.

References

- [1] Murray, C. B.; Norris, D. J.; Bawendi, M. G. Synthesis and Characterization of Nearly Monodisperse CdE (E = S, Se, Te) Semiconductor Nanocrystallites. *Journal of the American Chemical Society* **1993**, *115*, 8706–8715.

- [2] Murray, C. B.; Kagan, C. R.; Bawendi, M. G. Synthesis and Characterization of Monodisperse Nanocrystals and Close-Packed Nanocrystal Assemblies. *Annual Review of Materials Science* **2000**, *30*, 545–610.
- [3] Park, J.; Joo, J.; Kwon, S. G.; Jang, Y.; Hyeon, T. Synthesis of monodisperse spherical nanocrystals. *Angewandte Chemie International Edition* **2007**, *46*, 4630–60.
- [4] Williamson, C. B.; Nevers, D. R.; Hanrath, T.; Robinson, R. D. Prodigious Effects of Concentration Intensification on Nanoparticle Synthesis: A High-Quality, Scalable Approach. *Journal of the American Chemical Society* **2015**, *137*, 15843–15851.
- [5] Owen, J.; Brus, L. Chemical Synthesis and Luminescence Applications of Colloidal Semiconductor Quantum Dots. *Journal of the American Chemical Society* **2017**, *139*, 10939–10943.
- [6] Shamsi, J.; Urban, A. S.; Imran, M.; De Trizio, L.; Manna, L. Metal Halide Perovskite Nanocrystals: Synthesis, Post-Synthesis Modifications, and Their Optical Properties. *Chemical Reviews* **2019**, *119*, 3296–3348.
- [7] Yin, Y.; Alivisatos, A. P. Colloidal nanocrystal synthesis and the organic-inorganic interface. *Nature* **2005**, *437*, 664–670.
- [8] Chen, Y.; Johnson, E.; Peng, X. Formation of Monodisperse and Shape-Controlled MnO Nanocrystals in Non-Injection Synthesis: Self-Focusing via Ripening. *Journal of the American Chemical Society* **2007**, *129*, 10937–10947.
- [9] Sugimoto, T. Underlying mechanisms in size control of uniform nanoparticles. *Journal of colloid and interface science* **2007**, *309*, 106–18.
- [10] Chu, D. B. K.; Owen, J. S.; Peters, B. Nucleation and Growth Kinetics from LaMer Burst Data. *The Journal of Physical Chemistry A* **2017**, *121*, 7511–7517.
- [11] Whitehead, C. B.; Watzky, M. A.; Finke, R. G. "Burst Nucleation" vs Autocatalytic, "Burst" Growth in Near-Monodisperse Particle-Formation Reactions. *The Journal of Physical Chemistry C* **2020**, *124*, 24543–24554.
- [12] Bealing, C. R.; Baumgardner, W. J.; Choi, J. J.; Hanrath, T.; Hennig, R. G. Predicting Nanocrystal Shape through Consideration of Surface-Ligand Interactions. *ACS Nano* **2012**, *6*, 2118–2127.
- [13] Barnard, A. S. Direct Comparison of Kinetic and Thermodynamic Influences on Gold Nanomorphology. *Accounts of Chemical Research* **2012**, *45*, 1688–1697.
- [14] Xia, Y.; Xia, X.; Peng, H.-C. Shape-Controlled Synthesis of Colloidal Metal Nanocrystals: Thermodynamic versus Kinetic Products. *Journal of the American Chemical Society* **2015**, *137*, 7947–7966.
- [15] Deryagin, B. V. The Stability of Colloid Systems (Theoretical Aspects). *Russian Chemical Reviews* **1979**, *48*, 363.
- [16] Beverly, K. C.; Sampaio, J. F.; Heath, J. R. Effects of Size Dispersion Disorder on the Charge Transport in Self-Assembled 2-D Ag Nanoparticle Arrays. *Journal of Physical Chemistry B* **2002**, *106*, 2131–2135.
- [17] Yang, J.; Wise, F. W. Effects of Disorder on Electronic Properties of Nanocrystal Assemblies. *The Journal of Physical Chemistry C* **2015**, *119*, 3338–3347.
- [18] Savitzky, B. H.; Hovden, R.; Whitham, K.; Yang, J.; Wise, F.; Hanrath, T.; Kourkoutis, L. F. Propagation of Structural Disorder in Epitaxially Connected Quantum Dot Solids from Atomic to Micron Scale. *Nano Letters* **2016**, *16*, 5714–5718.
- [19] Reich, K. V. Conductivity of quantum dot arrays. *Physics-Uspokhi* **2020**, *63*, 994.
- [20] Stoeva, S.; Klabunde, K. J.; Sorensen, C. M.; Dragieva, I. Gram-Scale Synthesis of Monodisperse Gold Colloids by the Solvated Metal Atom Dispersion Method and Digestive Ripening and Their Organization into Two- and Three-Dimensional Structures. *Journal of the American Chemical Society* **2002**, *124*, 2305–2311.

- [21] Vayssières, L. On the thermodynamic stability of metal oxide nanoparticles in aqueous solutions. *International Journal of Nanotechnology* **2005**, *2*, 411.
- [22] Vayssières, L.; Chanéac, C.; Tronc, E.; Jolivet, J. P. Size Tailoring of Magnetite Particles Formed by Aqueous Precipitation: An Example of Thermodynamic Stability of Nanometric Oxide Particles. *Journal of Colloid and Interface Science* **1998**, *205*, 205–212.
- [23] Stoeva, S. I.; Zaikovski, V.; Prasad, B. L. V.; Stoimenov, P. K.; Sorensen, C. M.; Klabunde, K. J. Reversible Transformations of Gold Nanoparticle Morphology. *Langmuir* **2005**, *21*, 10280–10283.
- [24] Lin, Z.; Gilbert, B.; Liu, Q.; Ren, G.; Huang, F. A Thermodynamically Stable Nanophase Material. *Journal of the American Chemical Society* **2006**, *128*, 6126–6131.
- [25] Pavlova-Verevkina, O. B.; Pertsov, A. V. Possibility of the Existence of Equilibrium Oxide Hydrosols. *Colloid Journal* **1995**, *57*, 869–870.
- [26] Smetana, A. B.; Klabunde, K. J.; Sorensen, C. M. Synthesis of spherical silver nanoparticles by digestive ripening, stabilization with various agents, and their 3-D and 2-D superlattice formation. *Journal of Colloid and Interface Science* **2005**, *284*, 521–526.
- [27] Shaik, A. H.; Chakraborty, J. Synthesis of monodisperse copper nanoparticles using a modified digestive ripening technique and formation of superlattices. *RSC Advances* **2015**, *5*, 85974–85977.
- [28] Cingarapu, S.; Yang, Z.; Sorensen, C. M.; Klabunde, K. J. Synthesis of CdSe Quantum Dots by Evaporation of Bulk CdSe using SMAD and Digestive Ripening Processes. *Chemistry of Materials* **2009**, *21*, 1248–1252.
- [29] Yoder, T. S.; Cloud, J. E.; Leong, G. J.; Molk, D. F.; Tussing, M.; Miorelli, J.; Ngo, C.; Kodambaka, S.; Eberhart, M. E.; Richards, R. M.; Yang, Y. Iron Pyrite Nanocrystal Inks: Solvothermal Synthesis, Digestive Ripening, and Reaction Mechanism. *Chemistry of Materials* **2014**, *26*, 6743–6751.
- [30] Kim, M.-G.; Jeong, J.; Choi, Y.; Park, J.; Park, E.; Cheon, C.-H.; Kim, N.-K.; Min, B. K.; Kim, W. Synthesis of V-doped In₂O₃ Nanocrystals via Digestive-Ripening Process and Their Electrocatalytic Properties in CO₂ Reduction Reaction. *ACS Applied Materials & Interfaces* **2020**,
- [31] Lin, X.; Sorensen, C.; Klabunde, K. Digestive Ripening, Nanophase Segregation and Superlattice Formation in Gold Nanocrystal Colloids. *Journal of Nanoparticle Research* **2000**, *2*, 157–164.
- [32] Lee, D.-K.; Park, S.-I.; Lee, J. K.; Hwang, N.-M. A theoretical model for digestive ripening. *Acta Materialia* **2007**, *55*, 5281–5288.
- [33] Shimpi, J. R.; Sidhaye, D. S.; Prasad, B. L. V. Digestive Ripening: A Fine Chemical Machining Process on the Nanoscale. *Langmuir* **2017**, *33*, 9491–9507.
- [34] Thomas, T.; Sethuraman, S.; Satyam, D.; Kumar, D.; Kannadasan, B.; Anderson, A.; Prashant, S.; Vijayakrishnan, R.; Khan, S.; Das, P.; Kumar, M.; Bisi, K.; Chinta, Y.; Talluri, B. Surface enthalpy driven size focussing trends: Predictive modelling for digestive ripening of spherical particles. *Applied Surface Science* **2018**, *448*, 248–253.
- [35] Reiss, H. Entropy-induced dispersion of bulk liquids. *Journal of Colloid and Interface Science* **1975**, *53*, 61–70.
- [36] Ruckenstein, E. The origin of thermodynamic stability of microemulsions. *Chemical Physics Letters* **1978**, *57*, 517–521.
- [37] Stol, R. J.; De Bruyn, P. L. Thermodynamic stabilization of colloids. *Journal of Colloid and Interface Science* **1980**, *75*, 185–198.
- [38] Burlakov, V.; Goriely, A. Thermodynamic limit for particle monodispersity: How narrow can a particle size distribution be? *EPL (Europhysics Letters)* **2017**, *119*, 50001.

- [39] Kegel, W. K.; Reiss, H. Theory of Vesicles and Droplet Type Microemulsions: Configurational Entropy, Size Distribution, and Measurable Properties. *Berichte der Bunsengesellschaft für physikalische Chemie* **1996**, *100*, 300–312.
- [40] Tolman, R. C. The Effect of Droplet Size on Surface Tension. *The Journal of Chemical Physics* **1949**, *17*, 333–337.
- [41] Manzanares, J. A.; Peljo, P.; Girault, H. H. Understanding Digestive Ripening of Ligand-Stabilized, Charged Metal Nanoparticles. *The Journal of Physical Chemistry C* **2017**, *121*, 13405–13411.
- [42] Leff, D. V.; Ohara, P. C.; Heath, J. R.; Gelbart, W. M. Thermodynamic Control of Gold Nanocrystal Size: Experiment and Theory. *The Journal of Physical Chemistry* **1995**, *99*, 7036–7041.
- [43] Zhuang, Z.; Peng, Q.; Zhuang, J.; Wang, X.; Li, Y. Controlled Hydrothermal Synthesis and Structural Characterization of a Nickel Selenide Series. *Chemistry – A European Journal* **2006**, *12*, 211–217.
- [44] Zheng, J.; Xue, X.; Li, D.; Zhao, Y. New evidence of a thermodynamically stable nanophase: CdS in 4 M KOH-tert-butanol solution. *CrystEngComm* **2015**, *17*, 1509–1512.
- [45] Hill, T. L. *An Introduction to Statistical Thermodynamics*; Addison-Wesley: Reading, Massachusetts, 1960.
- [46] Volmer, M. Zur Theorie der lyophilen Kolloide. *Zeitschrift für Physikalische Chemie* **1927**, *125U*, 151–157.
- [47] Farkas, L. Keimbildungsgeschwindigkeit in übersättigten Dämpfen. *Zeitschrift für Physikalische Chemie* **1927**, *125U*, 236–242.
- [48] Avrami, M. Kinetics of phase change. I. General theory. *The Journal of Chemical Physics* **1939**, *7*, 1103–1112.
- [49] Lothe, J.; Pound, G. M. Reconsiderations of Nucleation Theory. *The Journal of Chemical Physics* **1962**, *36*, 2080–2085.
- [50] Nishioka, K.; Pound, G. M. Statistical mechanics of homogeneous nucleation in vapor. *Advances in Colloid and Interface Science* **1977**, *7*, 205–278.
- [51] Kelton, K. F. In *Solid State Physics*; Ehrenreich, H., Turnbull, D., Eds.; Academic Press, 1991; Vol. 45; pp 75–177.
- [52] Oxtoby, D. W. Homogeneous nucleation: theory and experiment. *Journal of Physics: Condensed Matter* **1992**, *4*, 7627–7650.
- [53] Reiss, H.; Kegel, W. K.; Katz, J. L. Resolution of the Problems of Replacement Free Energy, $1/S$, and Internal Consistency in Nucleation Theory by Consideration of the Length Scale for Mixing Entropy. *Physical Review Letters* **1997**, *78*, 4506–4509.
- [54] Vosel, S. V.; Onischuk, A. A.; Purtov, P. A. Translation-rotation correction factor in the theory of homogeneous nucleation. *The Journal of Chemical Physics* **2009**, *131*, 204508.
- [55] Lutsko, J. F. How crystals form: A theory of nucleation pathways. *Science Advances* **2019**, *5*, eaav7399.
- [56] Gebauer, D.; Cölfen, H. Prenucleation clusters and non-classical nucleation. *Nano Today* **2011**, *6*, 564–584.
- [57] Lee, J.; Yang, J.; Kwon, S. G.; Hyeon, T. Nonclassical nucleation and growth of inorganic nanoparticles. *Nature Reviews Materials* **2016**, *1*, 16034–16034.
- [58] Jehannin, M.; Rao, A.; Cölfen, H. New Horizons of Nonclassical Crystallization. *Journal of the American Chemical Society* **2019**, *141*, 10120–10136.

- [59] Whitehead, C. B.; Özkar, S.; Finke, R. G. LaMer’s 1950 Model for Particle Formation of Instantaneous Nucleation and Diffusion-Controlled Growth: A Historical Look at the Model’s Origins, Assumptions, Equations, and Underlying Sulfur Sol Formation Kinetics Data. *Chemistry of Materials* **2019**, *31*, 7116–7132.
- [60] Whitehead, C. B.; Özkar, S.; Finke, R. G. LaMer’s 1950 Model of Particle Formation: a Review and Critical Analysis of Its Classical Nucleation and Fluctuation Theory Basis, of Competing Models and Mechanisms for Phase-Changes and Particle Formation, and Then of Its Application to Silver Halide, Semiconductor, Metal, and Metal-Oxide Nanoparticles. *Materials Advances* **2021**, *2*, 186–235.
- [61] Reiss, H.; Katz, J. L. Resolution of the Translation-Rotation Paradox in the Theory of Irreversible Condensation. *The Journal of Chemical Physics* **1967**, *46*, 2496–2499.
- [62] Reiss, H.; Kegel, W. K. Replacement Free Energy and the $1/S$ Factor in Nucleation Theory as a Consequence of Mixing Entropy. *The Journal of Physical Chemistry* **1996**, *100*, 10428–10432.
- [63] Hill, T. L. *Thermodynamics of Small Systems*; Dover: Mineola, New York, 1994.
- [64] Hill, T. L.; Chamberlin, R. V. Extension of the thermodynamics of small systems to open metastable states: An example. *Proceedings of the National Academy of Sciences* **1998**, *95*, 12779–12782.
- [65] Rusanov, A. I. Thermodynamics of solid surfaces. *Surface Science Reports* **1996**, *23*, 173–247.
- [66] Kramer, D.; Weissmüller, J. A note on surface stress and surface tension and their interrelation via Shuttleworth’s equation and the Lippmann equation. *Surface Science* **2007**, *601*, 3042–3051.
- [67] Nanda, K. K.; Maisels, A.; Kruis, F. E. Surface Tension and Sintering of Free Gold Nanoparticles. *The Journal of Physical Chemistry C* **2008**, *112*, 13488–13491.
- [68] Nagarajan, R.; Ruckenstein, E. Molecular Theory of Microemulsions. *Langmuir* **2000**, *16*, 6400–6415.
- [69] Reiss, H.; Katz, J. L.; Cohen, E. R. Translation–Rotation Paradox in the Theory of Nucleation. *The Journal of Chemical Physics* **1968**, *48*, 5553–5560.
- [70] Kusaka, I. Statistical mechanics of nucleation: Incorporating translational and rotational free energy into thermodynamics of a microdroplet. *Physical Review E* **2006**, *73*, 031607.
- [71] Lothe, J.; Pound, G. M. On the Statistical Mechanics of Nucleation Theory. *The Journal of Chemical Physics* **1966**, *45*, 630–634.
- [72] Syneček, V.; Chessin, H.; Simerska, M. The temperature dependence of lattice vibrations in gold from X-ray diffraction measurements. *Acta Crystallographica Section A: Crystal Physics, Diffraction, Theoretical and General Crystallography* **1970**, *26*, 108–113.
- [73] Koenitzer, J. W.; Keesom, P. H.; Honig, J. M. Heat capacity of magnetite in the range 0.3 to 10 K. *Physical Review B* **1989**, *39*, 6231–6233.
- [74] Meroni, A.; Pimpinelli, A.; Reatto, L. On the entropy of mixing of a binary mixture of hard spheres. *The Journal of Chemical Physics* **1987**, *87*, 3644–3646.
- [75] Lichtenthaler, R. N.; Abrams, D. S.; Prausnitz, J. M. Combinatorial Entropy of Mixing for Molecules Differing in Size and Shape. *Canadian Journal of Chemistry* **2011**,
- [76] Sirota, E. B.; Rangwalla, H.; Peczak, P. Entropy of Mixing: Rigid vs Flexible Molecules: Effect of Varying Solvent on Dissolution Temperature. *Macromolecules* **2012**, *45*, 5281–5295.
- [77] Mansoori, G. A.; Carnahan, N. F.; Starling, K. E.; Leland, T. W. Equilibrium Thermodynamic Properties of the Mixture of Hard Spheres. *The Journal of Chemical Physics* **1971**, *54*, 1523–1525.
- [78] Salacuse, J. J.; Stell, G. Polydisperse systems: Statistical thermodynamics, with applications to several models including hard and permeable spheres. *The Journal of Chemical Physics* **1982**, *77*, 3714–3725.

- [79] Lin, X. M.; Wang, G. M.; Sorensen, C. M.; Klabunde, K. J. Formation and Dissolution of Gold Nanocrystal Superlattices in a Colloidal Solution. *The Journal of Physical Chemistry B* **1999**, *103*, 5488–5492.
- [80] Kamysbayev, V.; Srivastava, V.; Ludwig, N. B.; Borkiewicz, O. J.; Zhang, H.; Ilavsky, J.; Lee, B.; Chapman, K. W.; Vaikuntanathan, S.; Talapin, D. V. Nanocrystals in Molten Salts and Ionic Liquids: Experimental Observation of Ionic Correlations Extending beyond the Debye Length. *ACS Nano* **2019**, *13*, 5760–5770.
- [81] Monego, D.; Kister, T.; Kirkwood, N.; Doblas, D.; Mulvaney, P.; Kraus, T.; Widmer-Cooper, A. When Like Destabilizes Like: Inverted Solvent Effects in Apolar Nanoparticle Dispersions. *ACS Nano* **2020**, *14*, 5278–5287.
- [82] Israelachvili, J. N. *Intermolecular and Surface Forces*, 3rd ed.; Academic Press: Waltham, MA, 2011.
- [83] Schapotschnikow, P.; Pool, R.; Vlugt, T. J. H. Molecular Simulations of Interacting Nanocrystals. *Nano Letters* **2008**, *8*, 2930–2934.
- [84] Bocquet, L.; Trizac, E.; Aubouy, M. Effective Charge Saturation in Colloidal Suspensions. *The Journal of Chemical Physics* **2011**, *117*, 8659–8664.
- [85] Whetten, R. L.; Gelbart, W. M. Nanocrystal Microemulsions: Surfactant-Stabilized Size and Shape. *The Journal of Physical Chemistry* **1994**, *98*, 3544–3549.
- [86] De Gennes, P. G.; Taupin, C. Microemulsions and the flexibility of oil/water interfaces. *The Journal of Physical Chemistry* **1982**, *86*, 2294–2304.
- [87] Łodziana, Z.; Topsøe, N.-Y.; Nørskov, J. K. A negative surface energy for alumina. *Nature Materials* **2004**, *3*, 289–293.
- [88] Volmer, M. Die kolloidale Natur von Flüssigkeitsgemischen in der Umgebung des kritischen Lösungspunktes I. *Zeitschrift für Physikalische Chemie* **1956**, *206O*, 181–193.
- [89] Tremaine, P. R.; LeBlanc, J. C. The solubility of magnetite and the hydrolysis and oxidation of Fe²⁺ in water to 300°C. *Journal of Solution Chemistry* **1980**, *9*, 415–442.
- [90] Dreier, T. A.; Ackerson, C. J. Radicals Are Required for Thiol Etching of Gold Particles. *Angewandte Chemie International Edition* **2015**, *54*, 9249–9252.
- [91] Sellers, H.; Ulman, A.; Shnidman, Y.; Eilers, J. E. Structure and binding of alkanethiolates on gold and silver surfaces: implications for self-assembled monolayers. *Journal of the American Chemical Society* **1993**, *115*, 9389–9401.
- [92] Smith, A. M.; Johnston, K.; Crawford, S.; Marbella, L.; Millstone, J. Ligand density quantification on colloidal inorganic nanoparticles. *Analyst* **2017**, *142*, 11–29.
- [93] Barlow, R. J. *Statistics: a guide to the use of statistical methods in the physical sciences*; John Wiley & Sons: New York, 1989.
- [94] Sahu, P.; Prasad, B. L. V. Time and Temperature Effects on the Digestive Ripening of Gold Nanoparticles: Is There a Crossover from Digestive Ripening to Ostwald Ripening? *Langmuir* **2014**, *30*, 10143–10150.
- [95] Helfrich, W. Elastic Properties of Lipid Bilayers: Theory and Possible Experiments. *Zeitschrift für Naturforschung C* **1973**, *28*, 693–703.
- [96] Shchukin, E. D.; Rebinder, P. A. Formation of New Surfaces in the Deformation and Destruction of a Solid in a Surface-Active Medium. *Colloid Journal of the USSR* **1958**, *20*, 601–609.
- [97] Wen, Z.; Zhao, M.; Jiang, Q. Size Range of Solid-Liquid Interface Energy of Organic Crystals. *The Journal of Physical Chemistry B* **2002**, *106*, 4266–4268.